

The star formation history of early-type galaxies as a function of mass and environment

M. S. Clemens,^{1*} A. Bressan,^{1,2} B. Nikolic,³ P. Alexander,⁴ F. Annibali²
and R. Rampazzo¹

¹*INAF-Osservatorio Astronomico di Padova, Vicolo dell'Osservatorio, 5, 35122 Padova, Italy*

²*SISSA-ISAS, International School for Advanced Studies, via Beirut 4, 34014 Trieste, Italy*

³*National Radio Astronomy Observatory, Green Bank, WV (GB) and Charlottesville, VA (CV), USA*

⁴*Astrophysics Group, Cavendish Laboratory, Madingley Road, Cambridge CB3 0HE*

Accepted 2006 May 5. Received 2006 May 3; in original form 2005 October 13

ABSTRACT

Using the third data release of the Sloan Digital Sky Survey (SDSS), we have rigorously defined a volume-limited sample of early-type galaxies in the redshift range $0.005 < z \leq 0.1$. We have defined the density of the local environment for each galaxy using a method which takes account of the redshift bias introduced by survey boundaries if traditional methods are used. At luminosities greater than our absolute r -band magnitude cut-off of -20.45 , the mean density of environment shows no trend with redshift. We calculate the Lick indices for the entire sample and correct for aperture effects and velocity dispersion in a model-independent way. Although we find no dependence of redshift or luminosity on environment, we do find that the mean velocity dispersion, σ , of early-type galaxies in dense environments tends to be higher than in low-density environments. Taking account of this effect, we find that several indices show small but very significant trends with environment that are not the result of the correlation between indices and velocity dispersion. The statistical significance of the data is sufficiently high to reveal that models accounting only for α -enhancement struggle to produce a consistent picture of age and metallicity of the sample galaxies, whereas a model that also includes carbon enhancement fares much better. We find that early-type galaxies in the field are younger than those in environments typical of clusters but that neither metallicity, α -enhancement nor carbon enhancement are influenced by the environment. The youngest early-type galaxies in both field and cluster environments are those with the lowest σ . However, there is some evidence that the objects with the largest σ are slightly younger, especially in denser environments.

Independent of environment both the metallicity and α -enhancement grow monotonically with σ . This suggests that the typical length of the star formation episodes which formed the stars of early-type galaxies decreases with σ . More massive galaxies were formed in faster bursts.

We argue that the timing of the process of formation of early-type galaxies is determined by the environment, while the details of the process of star formation, which has built up the stellar mass, are entirely regulated by the halo mass. These results suggest that the star formation took place *after* the mass assembly and favours an anti-hierarchical model. In such a model, the majority of the mergers must take place before the bulk of the stars form. This can only happen if there exists an efficient feedback mechanism which inhibits the star formation in low-mass haloes and is progressively reduced as mergers increase the mass.

Key words: galaxies: abundances – galaxies: elliptical and lenticular, cD – galaxies: evolution.

*E-mail: marcel.clemens@oapd.inaf.it

1 INTRODUCTION

Present-day spheroids are thought to contain a large fraction, $\simeq 60$ – 80 per cent, of the total stellar mass in the Universe (Fukugita & Peebles 2004). They are thus fundamental tracers of the assembly of baryonic matter in the different environments generated from primordial density fluctuations.

There are well-established scaling relations indicating that the gravitational potential well is one of the key drivers in the formation and evolution of these galaxies. Suffice here to recall the colour–magnitude relation of early-type galaxies in clusters (Bower, Lucey & Ellis 1992), the relation between colour and central velocity dispersion and the Fundamental Plane (Bender, Burstein & Faber 1993). In contrast, the role played by the environment is not yet clear.

The environment may affect galaxy properties in two distinct ways: first, the initial conditions from which galaxies form are different, and secondly, their subsequent evolution may be affected by processes whose efficiency depends on environment.

As for the initial conditions, the hierarchical clustering paradigm predicts a very simple dependence on environment, in the sense that objects in denser regions form earlier (Lacey & Cole 1994). Subsequently, the environment (whether we mean the local galaxy density or membership of a cluster) may affect galaxy properties in several ways.

In galaxy clusters, the large-scale gravitational potential is directly responsible for so-called ‘galaxy harassment’ which describes the cumulative effects of high-speed encounters on the dynamics and star formation rate of the galaxies (Moore et al. 1996). Furthermore, the intracluster medium can remove high filling factor interstellar medium from disc galaxies (Gunn & Gott 1972). Initial conditions and subsequent environmental effects are the most likely explanations for the existence of the colour–magnitude relation (Bower et al. 1992), and the morphology–density relation (Dressler 1980; Balogh et al. 2004; Hogg et al. 2004; McIntosh, Rix & Caldwell 2004; Croton et al. 2005), respectively.

In the field, however, the separation of the different aspects of the environmental influence is rendered much less clear by the observational difficulty of obtaining homogeneous samples. Various authors, using samples of ~ 100 galaxies, found evidence that early-type galaxies in low-density environments are younger and more metal rich than those in clusters (Longhetti et al. 2000; Denicoló et al. 2005; Thomas et al. 2005). Several authors (e.g. Kuntschner et al. 2002; Denicoló et al. 2005; Thomas et al. 2005) also found that more massive and older galaxies have increased $[\alpha/\text{Fe}]$ values, suggesting more rapid star formation time-scales. Sánchez-Blázquez et al. (2003) used a sample of 98 galaxies to find lower C4668 and CN2 index values in the centre of the Coma cluster than in the field.

However, large and homogeneous galaxy samples are needed to provide the statistical discrimination necessary to identify small changes among stellar populations. Surveys such as the 2dF Galaxy Redshift Survey, Las Campanas Redshift Survey and the ongoing Sloan Digital Sky Survey (SDSS) have all been used for such studies. A sample of 1823 galaxies (of all types) has been used by Balogh et al. (1999) to find stronger 4000-Å break, and weaker $[\text{O II}]$ and $\text{H}\delta$ indices in the cluster environment. These authors concluded that the last star formation episode occurred more recently in low-density environments. Bernardi et al. (1998), with a sample 931 early-type galaxies found only a minimal difference in the $\text{Mg}2$ – σ relation, implying that field galaxies are only approximately 1 Gyr younger than those in clusters.

Bernardi et al. (2005) have used a sample of over 39 000 galaxies from the SDSS to find that age correlates with velocity dispersion

from an analysis of the colour–magnitude–velocity dispersion relation. Based on a similar sample Bernardi et al. (2006) analysed Lick indices to conclude that early-type galaxies in dense environments are less than 1 Gyr older than field objects and have a similar metallicity. Similar results have also been obtained by Smith et al. (2006) and Nelan et al. (2005).

In this paper, we study the absorption-line indices of a large sample of early-type galaxies selected from the third data release of the SDSS. We couple the high statistical significance of the sample with the most recent stellar population models to obtain an unbiased picture of the history of star formation in spheroids, as a function of their velocity dispersion, in different environments.

This paper is organized as follows. Section 2 is devoted to the sample selection and definition of environment. In Section 3, we derive the narrow-band indices and describe the various corrections to transform them to the Lick IDS (Image Dissector Scanner) system. In Section 4, we analyse the data by means of our new simple stellar population (SSP) models. Our findings are discussed in Section 5. Finally, in the conclusion section, we present an evolutionary scenario as a function of galaxy mass and environment.

2 THE SAMPLE AND DATA

2.1 Sample selection

The primary sample used in this study was selected along similar lines to the sample used by Gómez et al. (2003) and Nikolic, Cullen & Alexander (2004), that is, it is a luminosity- and (pseudo) volume-limited sample. The parent sample consisted of all objects, as of Data Release 3 (DR3), observed spectroscopically by the SDSS and classified as galaxies.¹ In practice, all the galaxies that are part of our sample, given its selection criteria, should have been selected for spectroscopic observations as a part of the SDSS Main Galaxy Sample (MGS) described by Strauss et al. (2002). Before selecting the volume-limited sample, a small number of spurious entries were identified and removed: galaxies within 5 arcsec of other galaxies (most likely deblending errors), galaxies with redshift confidence of less than 0.7 (they cannot be reliably placed in the volume-limited sample), and galaxies with z -band magnitudes fainter than 22.8, that is, not reliably detected in the z -band (these are most likely spurious detections).

The volume-limited sample was then constructed by selecting galaxies in the redshift range $0.005 < z \leq 0.1$ and with Petrosian absolute magnitudes brighter than -20.45 . Since the r -band magnitude limit of the MGS is 17.7, the absolute magnitude limit adopted should avoid a Malmquist bias in the volume-limited sample.

In order to limit our sample to include only early-type galaxies, we then adopted the following selection procedure. (i) The compactness ratio as defined in the SDSS was constrained to be less than 0.33 (see Shimasaku et al. 2001). (ii) Any object with detected emission in the $\text{H}\alpha$ line was excluded in order to minimize the effects of Balmer emission-line infilling. This is particularly important for the correct interpretation of the $\text{H}\beta$ absorption feature. To this sample, we further restricted the objects of study to (iii) those objects with a well-measured velocity dispersion, and (iv) those objects where the density of the environment could be well determined, independently of survey boundaries (see below). After such selection, our sample consisted of 3614 galaxies. In Section 4.3, we describe a further

¹ These are all the objects in files `gals-DR2.fit.gz` and `gals-DR3.fit.gz`, available at http://das.sdss.org/DR3/data/spectro/ss_tar_23/.

selection based on the signal-to-noise ratio (S/N) of the spectra to be included in the final regression analysis.

2.2 Estimating density of environment

The algorithm used to quantify the density of the environment is similar to that used by Dressler (1980) in his original study of the relationship between density and morphology: it is based on finding the projected separation to the n th nearest neighbour, r_n . This distance can, if required, be used to estimate the surface density of galaxies via $\sigma_{D,n} = n/r_n^2 \pi$.

Unlike the original algorithm, the one presently employed makes use of the measured redshifts of galaxies to search for nearest neighbours only in the redshift shell $\Delta v = \pm 1200 \text{ km s}^{-1}$ around the galaxy being considered following Gómez et al. (2003) and Goto et al. (2003) (although our maximum velocity difference is slightly larger). Because of this modification, no correction for the background galaxy field density needs to be made. Since in our approach redshift information is required, the search for n th nearest neighbour is necessarily restricted to a sample of galaxies with measured redshifts. To avoid a dependence of the calculated density scale on redshift, we search for n th nearest neighbour in the volume-limited catalogue itself. A photometric approach to calculating galaxy density in the SDSS is discussed by Hogg et al. (2003).

Since density of environment is a non-local measure, survey boundaries will inevitably present a problem. Galaxies close to one of the boundaries will have the separation to their n th neighbour (the density metric that we are using in this study) overestimated and therefore their density of environment underestimated; this effect is quite clearly illustrated in the simulations presented by Miller et al. (2003). Hence galaxies close to survey edges have unreliably measured densities and should not be considered in further analysis. The non-compact nature of the SDSS survey area makes this effect quite pronounced, although less so in DR3 than in earlier releases.

The usual approach to dealing with this problem is to remove from further analysis galaxies with n th neighbours at a larger separation than a survey boundary. This was shown by Miller et al. (2003) to be effective, but such an approach also preferentially removes galaxies in low-density environments at low redshift compared to high redshift, as shown in the upper panel of Fig. 1. This can be understood by considering a population of galaxies with a fixed physical distance to their n th neighbour: with increasing redshift, the *angular* separation to a survey boundary can be smaller and still allow good estimation of density; therefore the necessary margin around the survey boundary decreases and the effective useful area of the survey increases with increasing redshift.

The correlation between density and redshift in the sample after such an edge-correction procedure can be avoided by removing a somewhat larger number of galaxies as follows. If r_n is the separation to the n th neighbour and r_E is the separation to a survey edge, only galaxies which satisfy $r_n \frac{z}{z_0} \leq r_E$ should be retained in the edge-corrected sample, where z_0 is a fiducial redshift which should also be (close to) the lower redshift limit of the sample.

Finally, the choice of n to use as a density metric will also determine how much of an effect survey boundaries have. We follow Goto et al. (2003) and use $n = 5$ throughout. The edge-corrected sample is shown in the lower panel of Fig. 1.

Fig. 2 shows the distribution of our measure of environment for all the galaxies in our sample.

In Fig. 3, we compare our measure of the local galaxy density with the number of cluster members for those Abell clusters where our sample contains at least one galaxy. There is a correlation be-

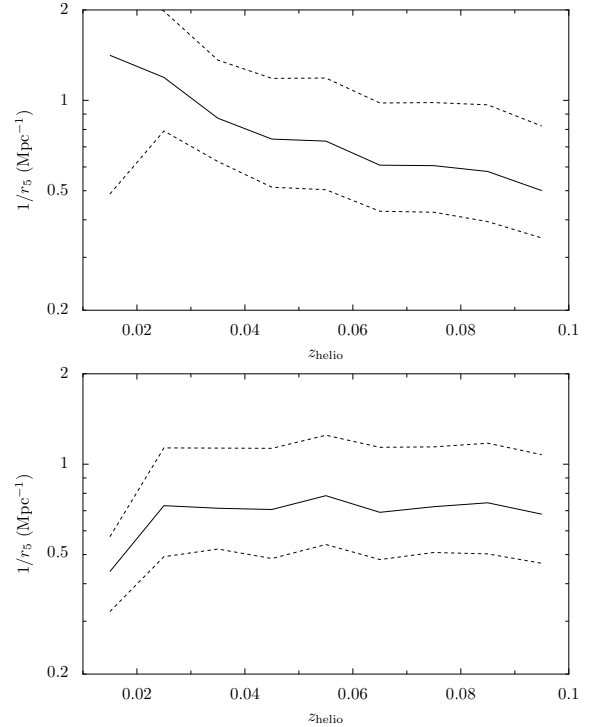


Figure 1. The distributions – represented as the median (solid line) and the 25 and 75 per cent quartiles (dashed lines) – of density as a function of redshift for samples corrected for the effects of survey boundaries in the traditional way (top panel) and using the technique described in the text (bottom panel).

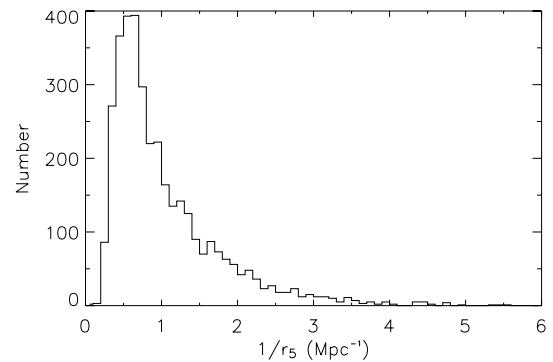


Figure 2. The distribution of the environmental density for our sample.

tween the measures but one is not a good predictor of the other, and neither would one especially expect them to be. Our measure of environment quantifies the *local* environment of a galaxy, whereas the total number of galaxies in an Abell cluster is a measure of the large-scale environment (recall also that we define environment using only those galaxies bright enough to be detected at all redshifts in our sample). The most important point about Fig. 3 is that it shows that galaxies in our sample that have a density parameter above 1 are in environments typical of galaxy clusters. Thirty-eight per cent of our galaxies have a value of $1/r_5 > 1.0$, and 10 per cent $1/r_5 > 2.0$.

As a further check for the reliability of our measure of environment, we visually checked the fields of our sample galaxies with the 20 highest and 20 lowest values of $1/r_5$. This confirmed that low

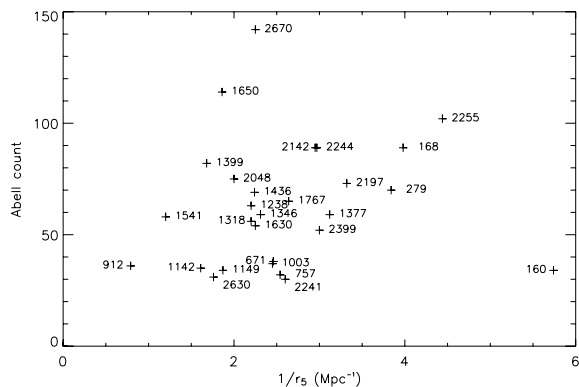


Figure 3. Comparison of our measure of environment, $1/r_5$, with the number of cluster members as given in Abell. The values of $1/r_5$ are the mean values for the galaxies in our sample associated with each cluster. The Abell cluster designation is shown near each point.

values do indeed represent galaxies in poor environments and vice versa.

3 CALCULATING THE LINE INDICES

Since one of the final goals of this study is to interpret the indices with models based on the Lick system, we first transform the SDSS spectra to the wavelength-dependent resolution of the Lick IDS spectra. This corresponds to $\sim 11.5 \text{ \AA}$ at 4000 \AA , $\sim 8.4 \text{ \AA}$ at 5000 \AA and $\sim 9.8 \text{ \AA}$ at 6000 \AA .

From the SDSS spectra, we then extract the 21 line-strength indices of the original Lick IDS system (Trager et al. 1998) plus the additional indices $H\gamma A$, $H\delta A$ and $H\gamma F$, $H\delta F$ (Worthey & Ottaviani 1997) and the indices B4000 (Hamilton 1985) and HK (Rose 1984, 1985). Our extraction makes use of the redshift of each object as provided in the SDSS. For this extended Lick system, we transform the passband definition of Trager et al. (1998) to the vacuum (SDSS spectra are given in terms of vacuum wavelengths). A comparison with the indices in common with the associated SDSS tables shows that they lie on a one-to-one relation.

In our analysis, the transformation to the Lick system, which is usually made by comparing selected observed standard stars with the Lick IDS observations, is not possible. This is simply because of the lack of observations of standard Lick stars in the adopted SDSS data release. For this reason, we work with index differences, that is, we do not consider absolute values but only trends with respect to a reference population. This strategy avoids significant biases in our analysis, because it has been shown that the transformations to the Lick IDS standard stars mostly consist of an offset correction (see e.g. Puzia et al. 2002; Rampazzo et al. 2005). Our results will also be much less dependent on the zero point calibration of the SSP models.

The errors on each index measurement were calculated by first measuring the rms noise in each spectrum and then reproducing a model spectrum with the same rms. We then used a Monte Carlo method to measure the indices for 200 realizations of the spectrum. We define the error on our measurement of an index as the standard deviation of the index values so obtained.

3.1 Velocity dispersion correction

Because we are interested in the intrinsic index– σ relation for early-type galaxies, it is important that no bias be introduced by an

inappropriate velocity dispersion correction. However, as we show in Appendix A, although most indices show some correlation with the velocity dispersion of a galaxy, and velocity dispersion is in turn correlated with environment, our results on the influence of the environment are not sensitive to our velocity dispersion correction. The velocity dispersion correction is thus important only for the shape of the index– σ relations. The velocity dispersion for each galaxy is provided in the SDSS.

To ensure that our derived index– σ relations are not a result of an error in velocity dispersion correction, we have made the correction in two different ways and carried out our analysis with both versions.

In the first, we simply smooth all the spectra to a velocity resolution of 400 km s^{-1} . Although this will result in index values which are all lower than they would be at, say, the resolution of the Lick system, we are sure that we have not introduced any model-dependent effects.

In the second method, we have smoothed the spectra of G- and K-type giant stars observed by the SDSS to a number of different velocity dispersions from zero to 400 km s^{-1} . For each index of a given galaxy, we identify a stellar spectrum with the same velocity dispersion and with similar line-index values, and then use this star to make the correction to the Lick IDS system.

A comparison between these two methods has been made by using the stars observed by the SDSS to correct indices to a velocity dispersion of 400 km s^{-1} and comparing to the results of the first method. Only in some of the bluer indices (Ca4227, G4300, Fe4383 and Ca4455) was any difference seen in the resulting index– σ relation.

3.2 Aperture correction

Every spectrum in the SDSS is taken through a fibre with a diameter of 3 arcsec and so the physical radius sampled for any given galaxy is a function of distance. We must apply an aperture correction to remove this effect. Rampazzo et al. (2005) have measured the spatial index gradients in 50 elliptical galaxies and we have used the mean radial gradients found for each index to correct our index values to the standard radius of $r_e/10$ where r_e is the effective radius. Using the data of Rampazzo et al., we take $[I(r_e/2) - I(r_e/10)]/I(r_e/10)$ as a measure of the spatial index gradient and plot this against $\log \sigma$ for all 50 galaxies in their sample. A least-squares, straight line fit to these plots is then found:

$$\frac{[I(r_e/2) - I(r_e/10)]}{I(r_e/10)} = x \log(\sigma/100) + y. \quad (1)$$

The values of x and y for each index are reported in Table 1. The SDSS gives values for the half light radius (r_e) of each galaxy and so we can correct the index measured with a 3-arcsec SDSS fibre to the standard radius of ($r_e/10$) by assuming a linear change in index value with radius:

$$I(r_e/10) = \frac{I(\text{SDSS})}{[x \log(\sigma/100) + y][\log(15/r_e)/\log 5] + 1}, \quad (2)$$

where $I(\text{SDSS})$, the index measured from the SDSS spectrum, is the index measured within a radius of 1.5 arcsec . σ is in units of km s^{-1} and r_e in arcseconds.

Fig. 4 shows the aperture corrections applied for each index. The accuracy of the aperture corrections depends on the accuracy of the value for the half light radius reported in the SDSS. This in turn will depend principally on the seeing. The fractional error will therefore increase with redshift, on average, as the angular size of the galaxies decreases, with the radii tending to be increasingly overestimated at greater distances. This effect has yet to be quantified in the current

Table 1. Parameter values for fits to the radial index variations measured by Rampazzo et al. (2005). Values for x and y in equation (1) are given.

Index	x	y	Index	x	y
CN1	0.468	-0.434	Fe5270	0.195	-0.0937
CN2	0.658	-0.463	Fe5335	0.0340	-0.0565
Ca4227	0.441	-0.0999	Fe5406	-0.0990	-0.0204
G4300	0.129	-0.0531	Fe5709	0.131	-0.0225
Fe4383	-0.0344	-0.0570	Fe5782	0.227	-0.0986
Ca4455	-0.111	-0.0716	NaD	0.127	-0.193
Fe4531	0.103	-0.0478	TiO1	0.143	-0.108
C4668	0.318	-0.219	TiO2	0.0434	-0.0573
H β	0.410	-0.0369	B4000	-0.0785	0.0574
Fe5015	0.517	-0.158	HK	0.0165	0.00396
Mg1	0.132	-0.142	HDF	1.18	-0.539
Mg2	0.131	-0.107	HGF	0.126	-0.183
Mgb	-0.0068	-0.0594			

release of the SDSS and the effect would influence the gradients of our index– σ plots (Fig. 5). However, as we see below, our derived index– σ relations agree very well with those derived from other studies based on more local samples and so we expect the influence of a seeing-induced effect to be small. Further, we note that because our various subsamples have similar redshift distributions (Fig. 6), our results on the influence of environment are insensitive to the gradient of the index– σ relations (see Appendix A).

4 RESULTS

Below we quantify our results making use of both simulations and models. We stress, however, that the results are qualitatively apparent in the data *before the use of either*. In the $\log\sigma$ –index plane, for example, several indices show a similar gradient for different environments but with an offset in index value. This immediately implies an effect of environment on the index that is not due to the elevated σ in denser environments (see Section 4.2). Because we have taken great care to minimize selection bias, we are able to treat the sample as a whole for the statistical analysis.

The velocity dispersion, σ , does not have a one-to-one relation to the mass of the galaxy. Recent work by Cappellari et al. (2006) has investigated the relation between galaxy mass-to-light ratio (M/L) and the line-of-sight component of the velocity dispersion within the effective radius. They provide relations (their equations 7 and 10) which allow a transformation from measured velocity dispersion to galaxy mass:

$$M_{10} = (16.5 \pm 7.8) \sigma_{200}^{3.11 \pm 0.43}, \quad (3)$$

where M_{10} is the galaxy mass in units of $10^{10} M_{\odot}$ and σ_{200} is the luminosity-weighted mean velocity dispersion within one effective radius in units of 200 km s^{-1} . The errors have been propagated from the parameter values found by Cappellari et al. (2006). We do not make any conversion to mass but those who wish to can apply this formula.

4.1 Trends of line indices with velocity dispersion

Fig. 5 shows the index– σ relations for our entire sample after the aperture and velocity dispersion corrections have been made. The gradients of the relations are reported for a simple first-order fit along

with the corresponding errors. Most indices show some correlation with the velocity dispersion.

The following indices show a significant ($> 5\sigma$) positive correlation: CN1, CN2, G4300, Fe4383, Ca4455, Fe4531, C4668, Mg1, Mg2, Mgb, Fe5335, Fe5406, NaD, TiO1, TiO2, (Fe), [Mg/Fe] (González 1993) and [Mg/Fe] defined as $\text{Mgb}/[0.5(\text{Fe } 5270 + \text{Fe } 5335)]$. Negative gradients are instead seen for: H β , H δ , H γ , Fe5015, B4000 (note the definition of this index in the SDSS is inverted with respect to that of many authors) and HK. No appreciable gradient is evident for: Ca4227, Fe5270, Fe5709 and Fe5782. Below we consider straight line fits of the form $I = a_0 + a_1 \log \sigma$ or $\log I = A_0 + A_1 \log \sigma$.

Most work on the trends of indices with velocity dispersion has been done for the Mg2– σ relation for which we find $a_1 = 0.209 \pm 0.0056$ and $a_0 = -0.198 \pm 0.013$. Bernardi et al. (1998) found $a_1 = 0.224 \pm 0.008$ and $a_0 = -0.23 \pm 0.019$ for a sample of 931 galaxies and Kuntschner et al. (2002) found corresponding values of 0.216 ± 0.025 and -0.236 ± 0.057 for Fornax spheroidals. Both studies gave fits consistent with ours. Jorgensen (1997) found values of $a_1 = 0.196 \pm 0.009$ and $a_0 = -0.155$. The slope is in agreement with our value, whereas the intercept seems to be slightly lower (although this author quotes no error on the intercept value).

For Mgb, we find $a_1 = 3.78 \pm 0.153$ ($A_1 = 0.389 \pm 0.0165$) which agrees well with Bernardi et al. (2003) and is similar to the relation found by Thomas, Maraston & Korn (2004) (although they did not explicitly quote the gradient).

For (Fe), we find $a_1 = 0.449 \pm 0.072$ and $a_0 = 1.78 \pm 0.162$ ($A_1 = 0.0820 \pm 0.0118$ and $A_0 = 0.258 \pm 0.0267$, respectively). These values are both consistent with those found by Bernardi et al. (2003) and Jorgensen (1997).

Our [Mg/Fe]– σ relation has $a_1 = 1.04 \pm 0.0700$, $a_0 = -0.747 \pm 0.159$ ($A_1 = 0.306 \pm 0.0194$, $A_0 = -0.499 \pm 0.044$). Kuntschner et al. (2002) found values in the range $A_1 \sim 0.18$ – 0.30 for < 100 early-type galaxies in Virgo, Coma and Fornax. Our value is consistent with their findings despite the fact that our value refers to early-type galaxies in a wide range of environments. Our [Mg/Fe]– σ relation is marginally consistent with that of Bernardi et al. (2003) who found $A_1 = 0.22 \pm 0.04$. Trager et al. (2000) found $A_1 = 0.33 \pm 0.01$ and $A_0 = -0.58 \pm 0.01$ which is similar to the gradient we find but with a slightly lower intercept.

We obtain a slope for the H β index of $a_1 = -1.75 \pm 0.0670$ ($A_1 = -0.450 \pm 0.0191$). This is similar to that found by Thomas et al. (2005) (~ -1.7) but is somewhat steeper than that found by Bernardi et al. (2003), who obtained $d(\log \text{H}\beta)/d(\log \sigma) = -0.24 \pm 0.03$.

A thorough treatment of the index– σ relations in cluster galaxies has been carried out by Nelan et al. (2005) (their table 7). Most of the gradients measured by these authors are similar to the gradients we find for our *high-density* subsample, but some indices show large differences from our measured trends. These are Ca4227, C4668, Fe5015 and Fe5270. We note that apart from the differences in sample characteristics, these authors applied an aperture correction to a fixed physical radius that is not a function of σ ; our correction instead is to $r_e/10$ and is applied as a function of velocity dispersion. Aperture corrections have not traditionally taken into account the fact that radial index gradients are a function of σ . We note that the indices in which we see the most significant disagreement tend to have aperture corrections that vary more strongly with σ (Fig. 4).

In Section 4.3, these relationships are interpreted in terms of physical parameters of the galaxies.

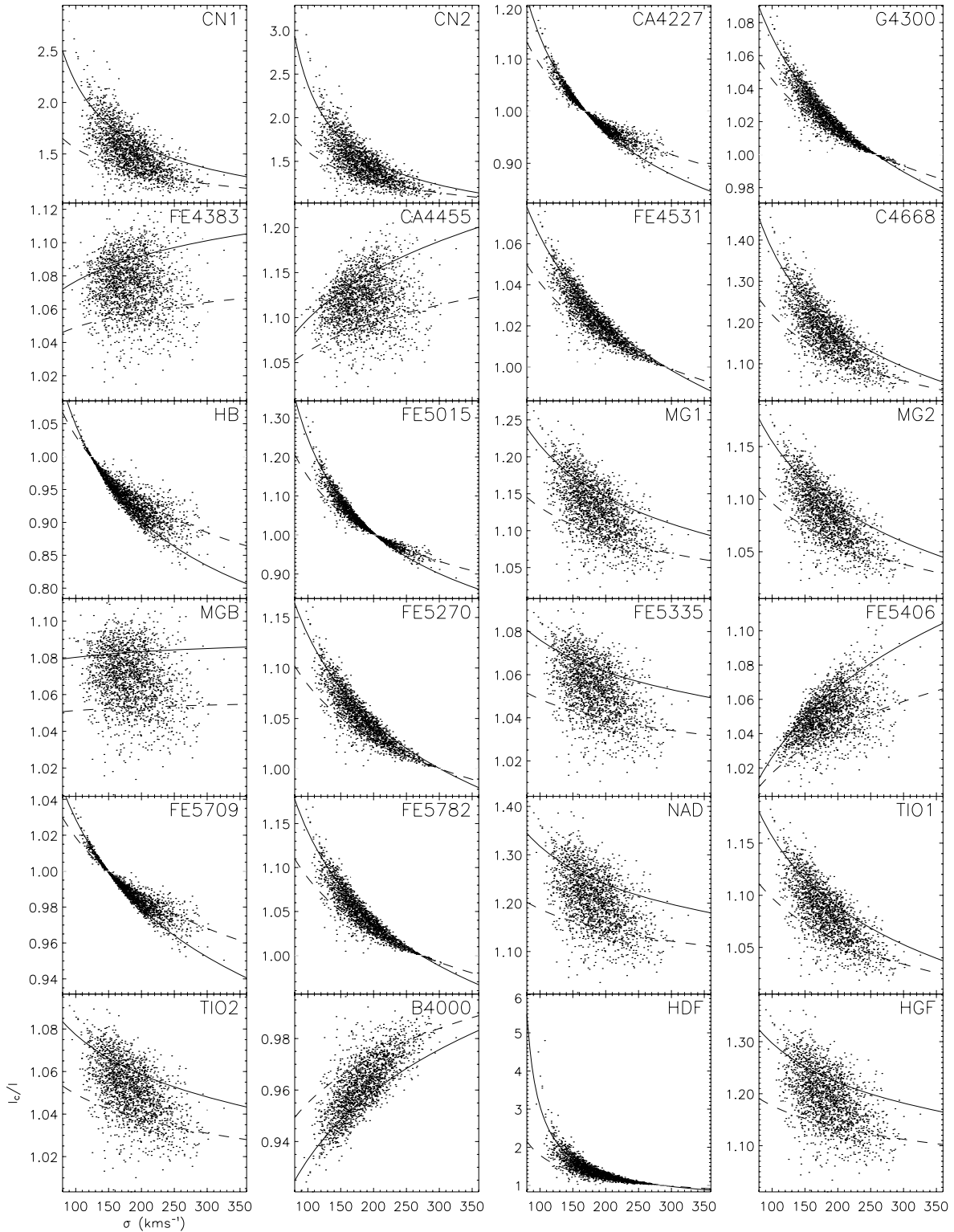


Figure 4. Aperture corrections as a function of velocity dispersion, σ . The points are the data, and the solid and dashed lines show the correction applied for an effective radius of 2 and 4 arcsec, respectively.

4.2 The effect of environment on the line indices

Having corrected our catalogue for the various biases discussed above, we then divided it in terms of the density parameter $1/r_5$ to investigate the effect of environment on the line indices. Of course,

if the distribution of our subsamples differs in any parameter that is correlated with the index, we must take account of this.

We divided our total sample of 3614 galaxies in the following way. First, we selected a low-density sample made up of those galaxies with $1/r_5 < 0.5$ (726 objects) against which to compare galaxies in

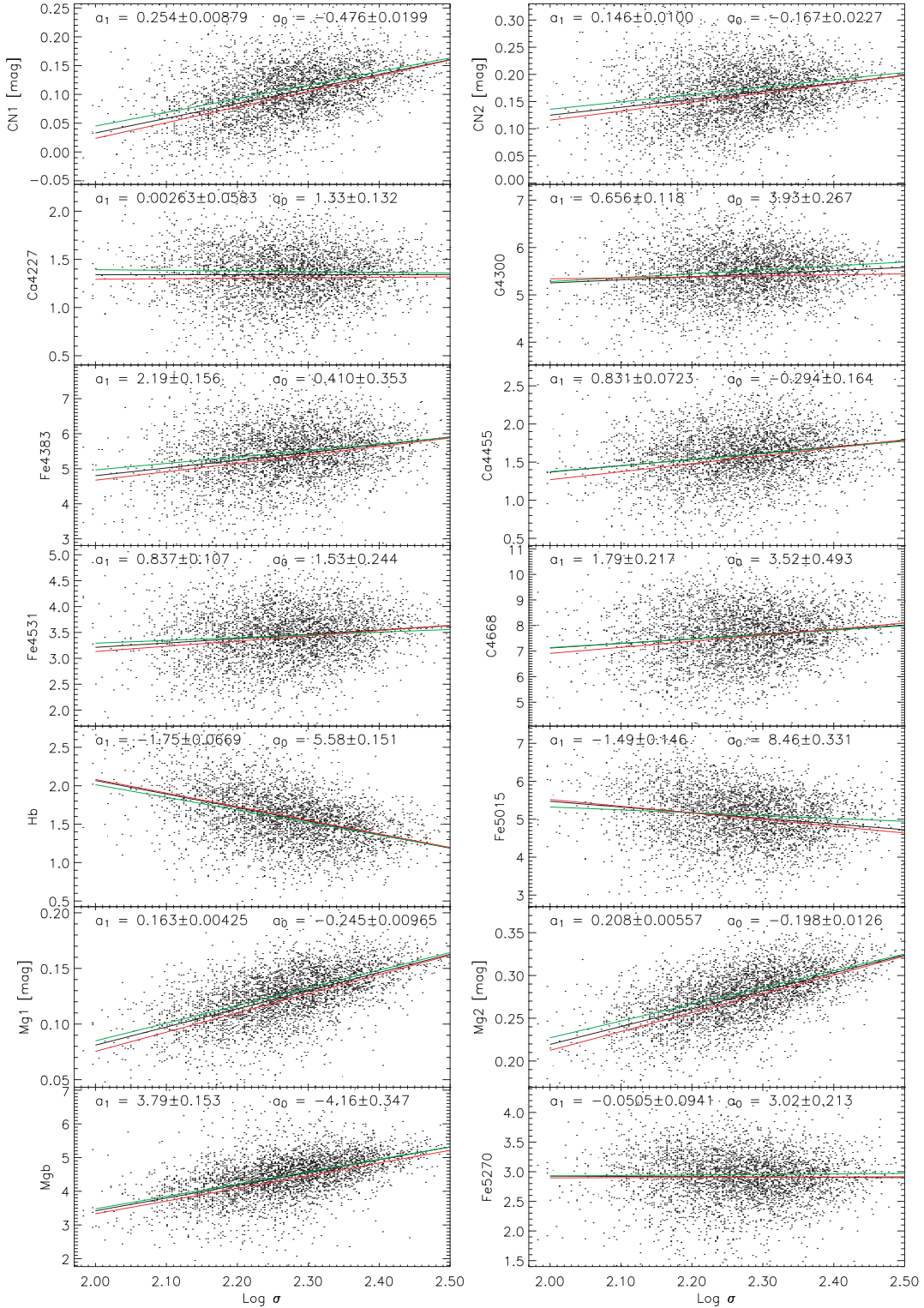


Figure 5. Index– σ relations. The data have been corrected for both aperture and velocity dispersion effects. The black line shows a least-squares, straight line fit to the whole sample, the parameters of which are reported at the top of each panel. The red and green lines show fits to low- and high-density subsamples with $1/r_5 < 0.5$ and $1/r_5 > 1.5$, respectively.

increasingly dense environments. These were then defined as follows: (i) $0.5 < 1/r_5 < 1.0$ (1513 objects), (ii) $1/r_5 > 0.5$ (2888 objects), (iii) $1/r_5 > 1.0$ (1362 objects), (iv) $1/r_5 > 1.5$ (706 objects), and (v) $1/r_5 > 2.0$ (357 objects). The upper density bound on

the first of these was intended to search for effects at environmental densities below those typical of clusters.

In Fig. 6, we show the distributions of velocity dispersion, redshift and luminosity for each of the subsamples compared with the

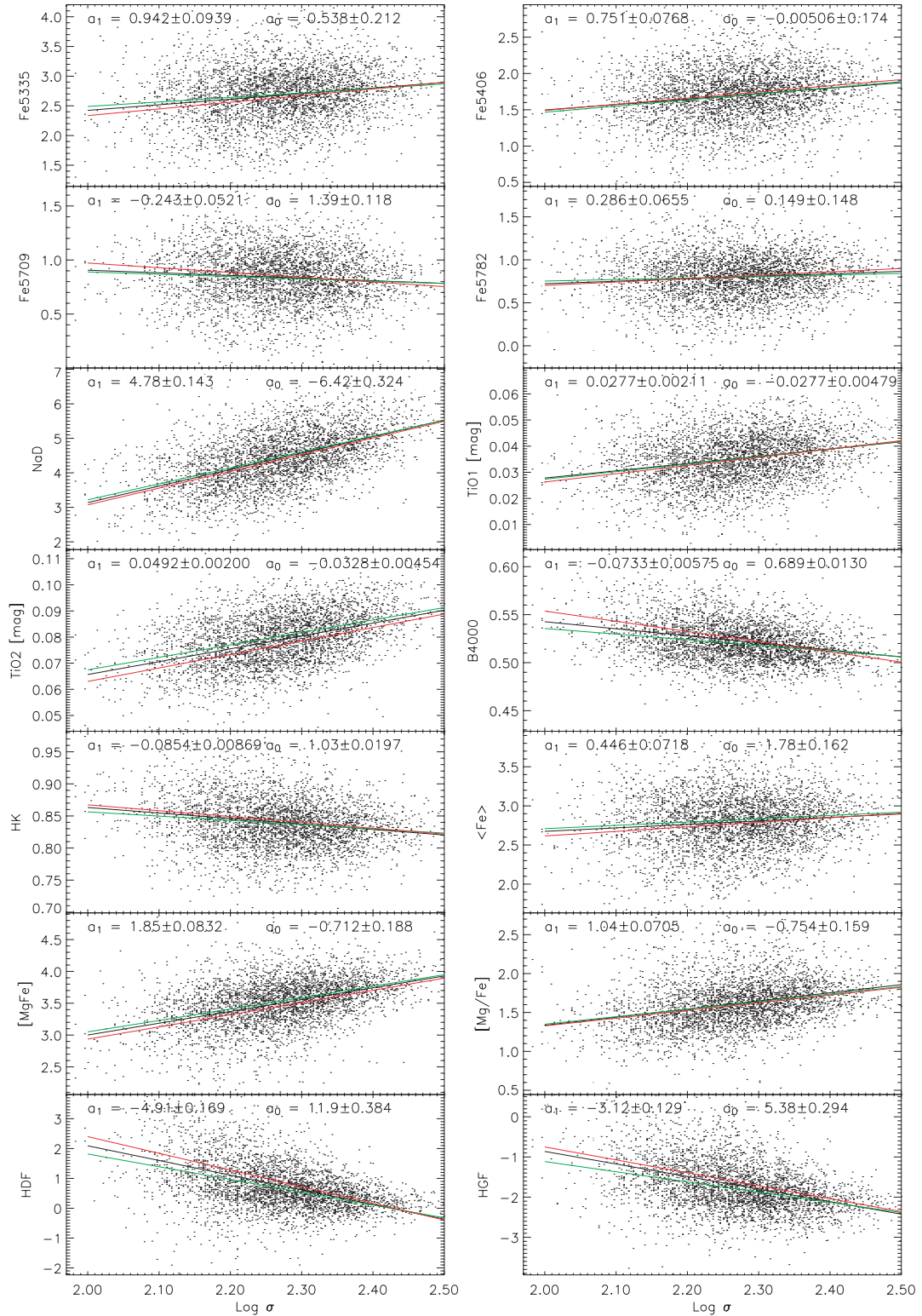


Figure 5 – continued

subsample with $1/r_5 < 0.5$ along with the probability that the two distributions are drawn from the same parent population. We note that the luminosity and redshift distributions are similar in each case (although the two lowest density bins for the redshift distribution have a probability of only 0.7 per cent of being drawn from

the same parent population, their means are similar). The distributions of velocity dispersion, on the other hand, are very significantly different in all cases. The velocity dispersion tends to be higher in denser environments and increases monotonically with our measure of the density of environment. At $1/r_5 < 0.5$, $\langle \sigma \rangle = 182.7 \text{ km s}^{-1}$,

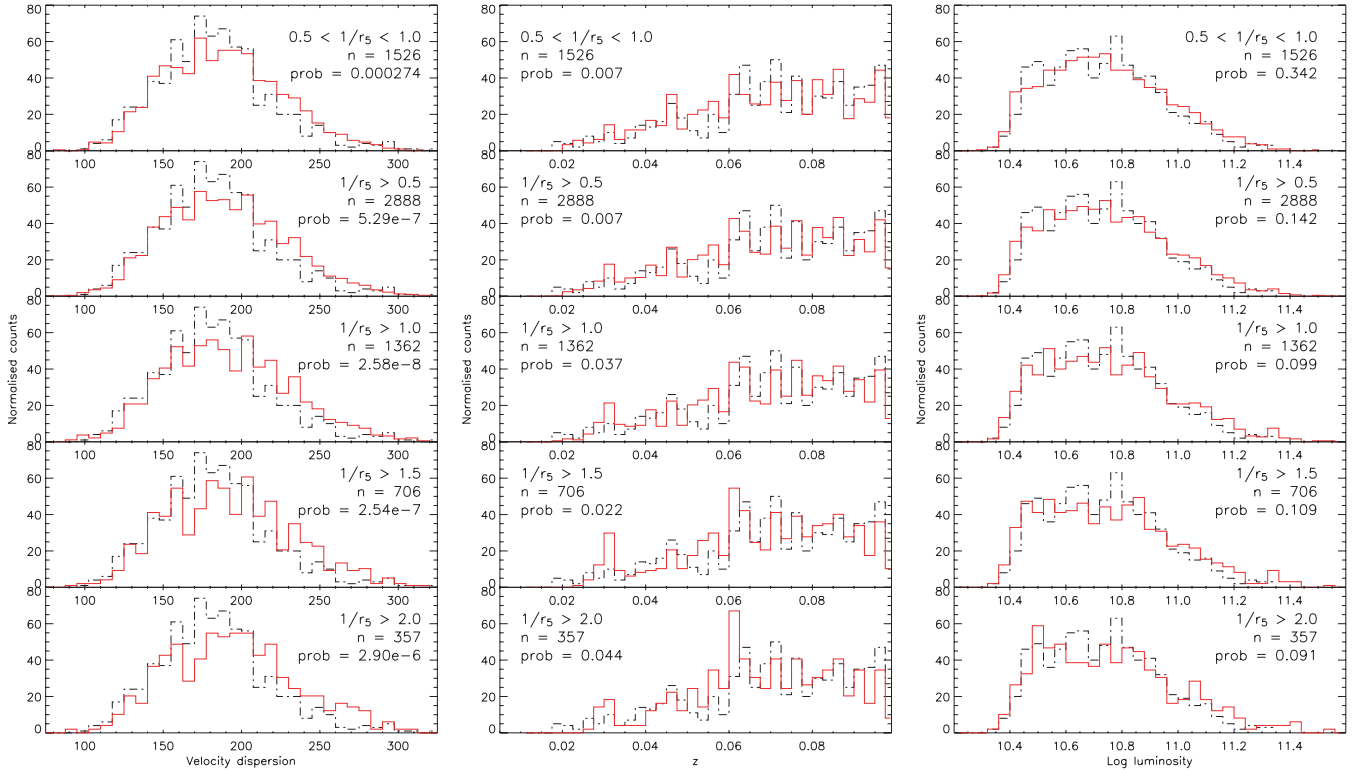


Figure 6. Distribution of velocity dispersion, redshift and z-band luminosity for various density environments. In each case, the dotted line is the distribution for the comparison subsample with $1/r_5 < 0.5$ and the solid (red) line is that for increasingly dense environments. Density increases from top to bottom in each panel. The density of the environment considered, number of galaxies, and the Kolmogorov–Smirnov (KS)-probability that the two distributions are drawn from the same parent population are shown in each plot. Left-hand panel: velocity dispersion, middle panel: redshift, right-hand panel: luminosity. The clear increase of the velocity dispersion with density of environment is quantified in Fig. 7

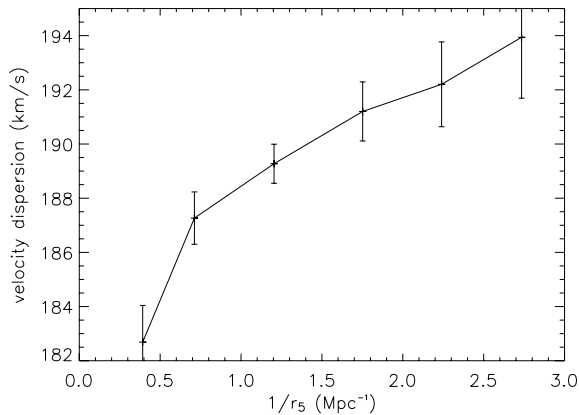


Figure 7. Mean value of the velocity dispersion, σ , as a function of our measure of the environmental density, $1/r_5$. The error bars are the standard deviations of the distribution of velocity dispersion divided by the square root of the number of objects.

whereas for $1/r_5 > 2.0$, $\langle \sigma \rangle = 193.9 \text{ km s}^{-1}$. This trend is illustrated in Fig. 7. In order to test that the differences in velocity dispersion distributions are not due to a special distribution in the subsample with $1/r_5 < 0.5$, we also compared each environment with the subsample with $0.5 < 1/r_5 < 1.0$. Significant differences remained (although at lower significance due to the smaller total number of objects and the smaller differences in $1/r_5$).

As we saw above, most indices show some correlation with the velocity dispersion. The differences in mean velocity dispersion for

different environments therefore mean that differences in the index values between environments will have a contribution due only to the index– σ relation. The two effects might entirely explain any index differences we find with environment. In order to take into account this effect, we have employed a Monte Carlo approach.

Using the entire sample (before defining regions in different environments), we consider the index– σ relation. Binning the data in σ with a bin width of 10 km s^{-1} , we plot the value of the mean index per bin against σ and linearly interpolate between points. This line is used to define the index– σ relation.

For a given subsample of environmental density, we then take the measured velocity dispersion value of each galaxy and translate it into a value for the index via the index– σ relation. In the process, we alter the derived index value by a random amount drawn from an appropriate Gaussian distribution so that the observed standard deviation of measured indices is correctly reproduced. We thus create a model data set with an index distribution defined only by the velocity dispersion of the subsample and the index– σ relation.

In this way, we generate a model index distribution for a given subsample of environmental density. Any difference between the index values from two model subsamples defined in this way is due only to the difference in the distribution of velocity dispersion. We quantify this difference by subtracting the means of two environmental density subsamples for 1000 realizations of the model. The distribution of this model difference gives us a distribution against which to test the observed difference in index. If the real data show a difference well in excess of that seen in the simulated data, then we identify an effect of environment on the index.

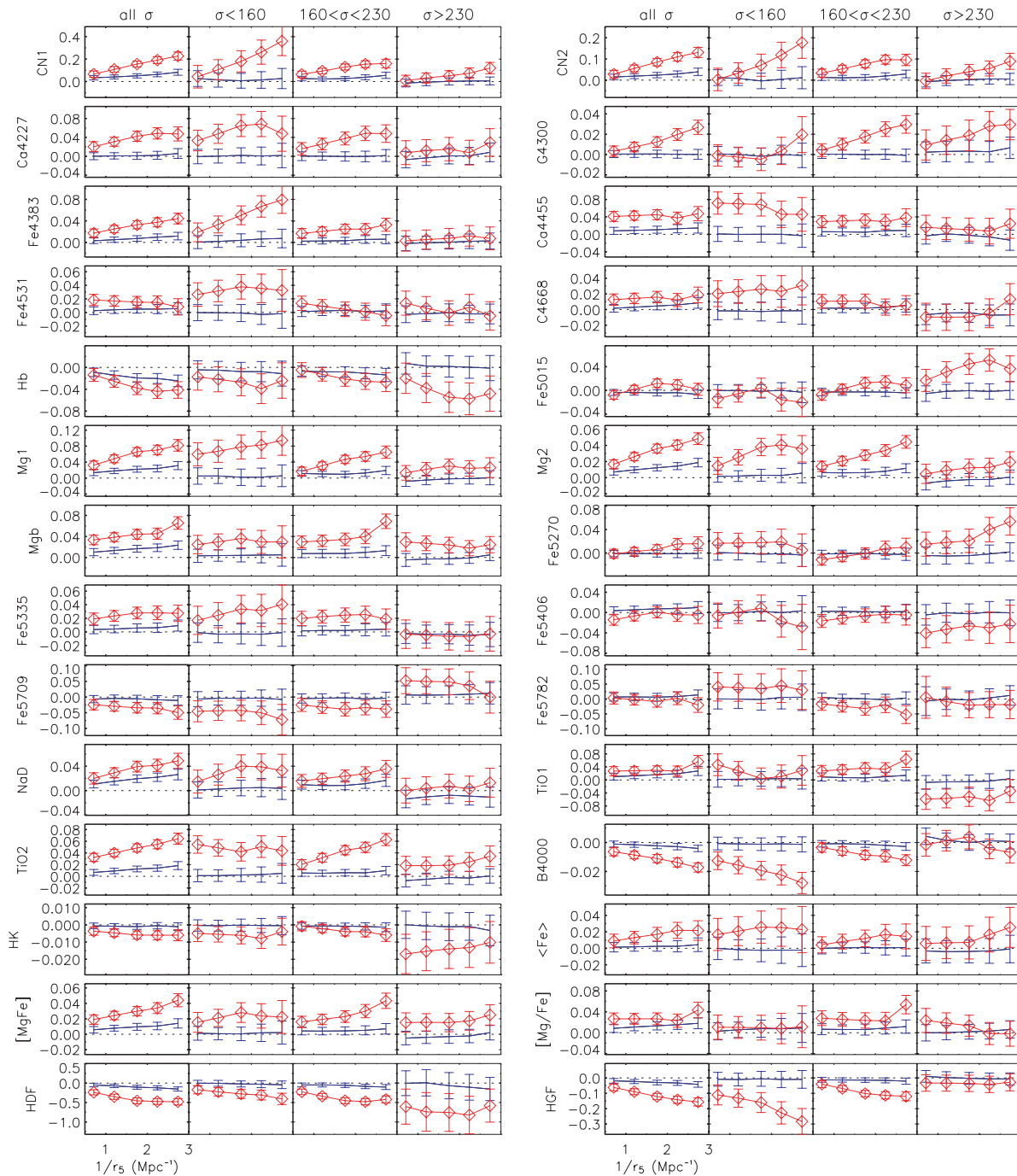


Figure 8. Comparison of normalized index values with the comparison low-density subsample ($1/r_5 < 0.5$) for increasingly dense environments. The horizontal axis shows values of the mean density of the environment ($1/r_5$) and the vertical axis shows the fractional deviation of the index value with respect to the sample mean. Vertical error bars show the results of Monte Carlo simulations which take into account the index– σ relation and the difference in the distribution of velocity distribution between environments of different density. The open diamonds represent the observed index difference. For each index, four panels are shown. The left-hand panel shows results for the whole sample. The other three panels show the results for three ranges of velocity dispersion. From left to right-hand panel: $\sigma < 160 \text{ km s}^{-1}$, $160 \leq \sigma \leq 230 \text{ km s}^{-1}$ and $\sigma > 230 \text{ km s}^{-1}$.

Fig. 8 displays the normalized index differences for five environments of increasing density, each compared to the subsample with the lowest density ($1/r_5 < 0.5$). The normalized index difference is given by

$$\Delta \langle I_s \rangle = \frac{\langle I_s \rangle - \langle I_0 \rangle}{\langle I \rangle} \quad (4)$$

where $\langle I_s \rangle$ is the mean value of the index in the subsample with mean environmental density s , $\langle I_0 \rangle$ is the mean value of the index in the comparison subsample and $\langle I \rangle$ is the mean index value for the whole sample over all environmental densities. Table 2 summarizes the results of Fig. 8.

The following indices show a statistically significant density dependence in the sense that index values are higher in more dense

Table 2. Comparison of normalized index values for the highest and lowest density subsamples shown in the left-hand panel of Fig. 8. The data and the simulation refer to the whole sample. LDE and HDE refer to densities of $1/r_5 = 0.712$ and $1/r_5 = 2.734$.

Index	Simulation LDE	Data LDE	Simulation HDE	Data HDE
CN1	0.034 ± 0.020	0.066 ± 0.028	0.083 ± 0.026	0.227 ± 0.036
CN2	0.015 ± 0.013	0.028 ± 0.018	0.039 ± 0.017	0.131 ± 0.024
Ca4227	0.000 ± 0.007	0.020 ± 0.010	0.006 ± 0.010	0.047 ± 0.015
G4300	0.000 ± 0.003	0.003 ± 0.005	0.000 ± 0.004	0.027 ± 0.007
Fe4383	0.003 ± 0.005	0.017 ± 0.007	0.012 ± 0.007	0.044 ± 0.010
Ca4455	0.008 ± 0.008	0.041 ± 0.011	0.015 ± 0.012	0.048 ± 0.016
Fe4531	0.003 ± 0.006	0.018 ± 0.008	0.006 ± 0.009	0.008 ± 0.012
C4668	0.002 ± 0.005	0.013 ± 0.007	0.009 ± 0.007	0.019 ± 0.010
H β	-0.009 ± 0.008	-0.014 ± 0.012	-0.025 ± 0.011	-0.041 ± 0.015
Fe5015	-0.003 ± 0.005	-0.008 ± 0.007	-0.007 ± 0.007	0.002 ± 0.010
Mg1	0.014 ± 0.007	0.032 ± 0.010	0.031 ± 0.0100	0.082 ± 0.014
Mg2	0.007 ± 0.004	0.017 ± 0.006	0.019 ± 0.005	0.048 ± 0.007
Mgb	0.010 ± 0.007	0.033 ± 0.009	0.023 ± 0.008	0.066 ± 0.012
Fe5270	-0.001 ± 0.005	-0.001 ± 0.008	-0.001 ± 0.008	0.016 ± 0.012
Fe5335	0.003 ± 0.006	0.019 ± 0.009	0.009 ± 0.008	0.027 ± 0.012
Fe5406	0.004 ± 0.008	-0.014 ± 0.011	0.010 ± 0.012	-0.005 ± 0.017
Fe5709	-0.006 ± 0.012	-0.025 ± 0.017	-0.011 ± 0.015	-0.050 ± 0.021
Fe5782	0.007 ± 0.014	0.003 ± 0.020	0.014 ± 0.017	-0.020 ± 0.025
NaD	0.011 ± 0.006	0.020 ± 0.009	0.026 ± 0.009	0.049 ± 0.012
TiO1	0.010 ± 0.010	0.027 ± 0.014	0.027 ± 0.014	0.056 ± 0.019
TiO2	0.007 ± 0.005	0.032 ± 0.007	0.018 ± 0.007	0.064 ± 0.009
B4000	-0.001 ± 0.002	-0.006 ± 0.003	-0.004 ± 0.002	-0.017 ± 0.003
HK	-0.001 ± 0.002	-0.004 ± 0.002	-0.001 ± 0.002	-0.006 ± 0.003
$\langle \text{Fe} \rangle$	0.001 ± 0.006	0.009 ± 0.008	0.004 ± 0.008	0.022 ± 0.012
[MgFe]	0.006 ± 0.004	0.019 ± 0.006	0.014 ± 0.006	0.044 ± 0.008
[Mg/Fe]	0.009 ± 0.008	0.027 ± 0.011	0.018 ± 0.010	0.044 ± 0.015
HdF	-0.048 ± 0.046	-0.237 ± 0.066	-0.152 ± 0.054	-0.480 ± 0.082
HgF	-0.019 ± 0.015	-0.062 ± 0.022	-0.042 ± 0.019	-0.157 ± 0.027

environments: CN1, CN2, Ca4227, G4300, Fe4383, (Ca4455), Mg1, Mg2, Mgb, (Fe5335) NaD, TiO2, and [MgFe] (parentheses indicate that we find an offset but not a trend with density). The B4000 index shows the opposite trend with lower values in more rich environments but this is simply due to how the index is defined in the SDSS. Although none of the differences attributable to environment significantly increase the scatter of index values of the population as a whole, the differences are very significant.

Indices which show an offset but no trend with density over the range of the plots of Fig. 8 show an excess of low values in the comparison low-density subsample.

The above indices have different sensitivities to age and metallicity variations and, in general, an increase of a metal index may indicate increased age and/or larger metallicity. As for the effects of the metallicity, we recall that the sensitivity to separate elemental variations is also important (enhancement) and has been investigated by various authors (Tripicco & Bell 1995; Trager et al. 1998; Thomas, Maraston & Bender 2003; Annibali et al. 2004; Korn, Maraston & Thomas 2005). Indeed, from the indices in which an effect is seen with density of environment (and from those which show little or no effect), we can also attempt to identify elemental abundance variations. In this respect, carbon is of particular importance.

Tripicco & Bell (1995) and Korn et al. (2005) showed that carbon has a strong influence on many of the indices in which we find a trend. However, it is striking that C4668, in spite of showing the greatest sensitivity to carbon, displays at most only a marginal increase with environmental density. This is inconsistent with an increase in carbon abundance being the cause of the differences we

see for these indices. It also suggests that, if a general abundance increase is the cause of the index difference, carbon is a bad tracer of overall abundance and that its relative abundance should decrease as metallicity increases.

We note that we do not reproduce the results of Sánchez-Blázquez et al. (2003) who found both a lower C4668 and CN2 index for early-type galaxies in the central regions of the Coma cluster when compared to the field. This study was based only on Coma galaxies and the mean environmental density of galaxies in our subsample with $1/r_5 \geq 1.5$ is unlikely to be as high as for those at the centre of the Coma cluster.

Besides the various dependencies of indices on elemental abundances, they are also, of course, affected by age. In order to make sense of the trends of the indices, we must make use of the sensitivity to the different physical parameters simultaneously.

4.3 Age, metallicity and α -enhancement

In order to extract trends in age, metallicity and α -enhancement from our measured trends in the line indices we have used the recent models computed by Annibali (PhD thesis and Annibali et al. 2004) and a multiple-linear regression analysis.

These models account for the effects of age, metallicity and α -enhancement variations. The models have been computed by adopting the fitting functions that describe the dependence of the Lick indices on stellar parameters. The effects of the element partition have been introduced following the sensitivity to different elements provided by Korn et al. (2005). In computing the effects

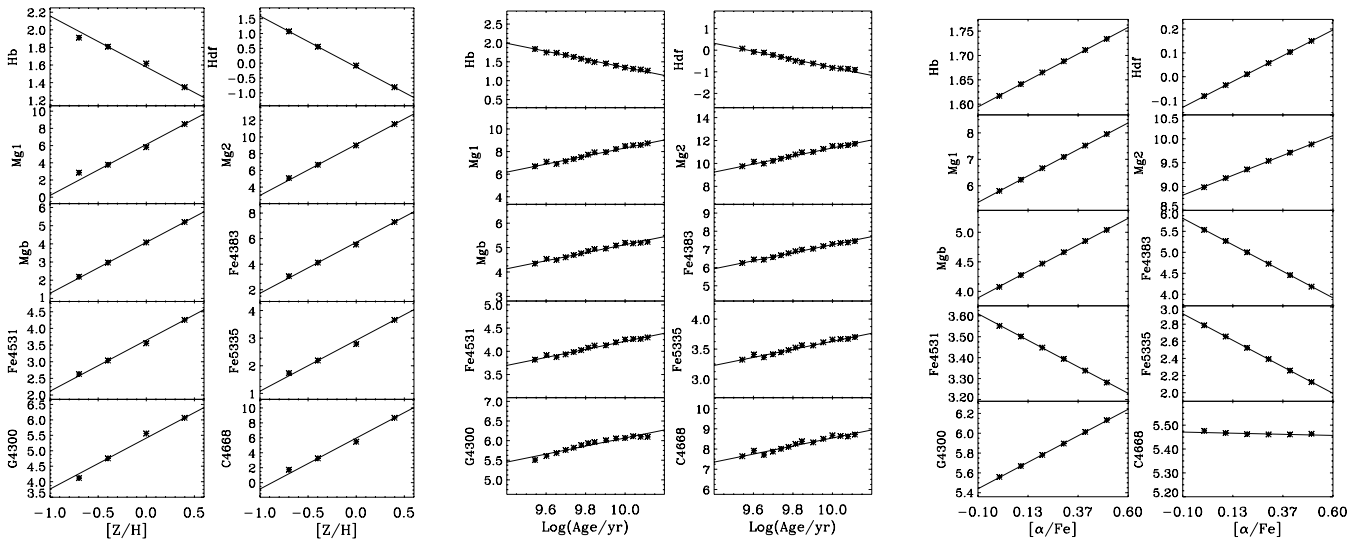


Figure 9. The linearity of our adopted models for the selected indices. Index variations versus, left-hand panel: metallicity [$\log(Z/Z_{\odot})$] at a fixed age of 10 Gyr and fixed $[\alpha/\text{Fe}]$ and $[\text{C}/\text{H}]$, middle panel: $\log(t)$, and right-hand panel: $[\alpha/\text{Fe}]$.

of α -enhancement, the elements N, O, Ne, Na, Mg, Si, S, Ca and Ti were assigned to the *enhanced* group, while Cr, Mn, Fe, Co, Ni, Cu and Zn to the *depressed* group. Because our analysis makes use of indices that show a mild to strong dependence on the relative abundance of carbon, we have also considered the effects of enhancing this element alone.

Our selection of indices to include in the regression analysis is restricted to those satisfying two criteria. First, the indices must be well modelled by the SSPs of Annibali et al. (2004), and secondly, those that have fractional errors < 20 per cent. In common with similar models by other workers (e.g. Thomas et al. 2003), certain indices are not reproduced well by the adopted SSP models. The CN indices are underpredicted compared with globular cluster data unless nitrogen is increased by a factor of 3 with respect to the α -elements. NaD is sensitive to interstellar absorption (Burstein et al. 1984) and so is of limited use for stellar population studies (Worthey et al. 1994). The model predictions of the Ca4227 index are slightly too high, while Ca4455 suffers from calibration problems (Maraston et al. 2003). The TiO1 and TiO2 indices appear to be poorly calibrated, and furthermore measured TiO1 indices may be affected by the presence of the broad NaD feature (Denicoló et al. 2005). Among the Fe indices, we adopted the classic Fe5270 and Fe5335 indices plus the blue Fe4383 and Fe4531 indices which are both sensitive to iron and well calibrated. The other iron indices are relatively poorly calibrated (Fe5782), are less sensitive to Fe (Fe5709), or may be affected by emission contamination (Fe5015, Kuntschner et al. 2002). For the age-sensitive indicators, we adopted the classic H β index, which is mostly independent of α -enhancement effects but may be affected by emission contamination and we preferred H δ to H γ as it is less affected by nebular emission.

Our final list of indices is: H β , H δ , Mg1, Mg2, Mgb, Fe4383, Fe4531, Fe5270, Fe5335, G4300 and C4668. (We note that the inclusion of H β has no significant effect on the results. The primary reason for its inclusion was to allow comparison with the results of other authors.) We find that our results are also not a strong function of the adopted S/N cut-off of the spectra.

We express the observed index variation as a linear combination of age, metallicity, α -enhancement and carbon variation:

$$\delta I = \frac{\partial I}{\partial \log(t)} \delta \log(t) + \frac{\partial I}{\partial \log(Z)} \delta \log(Z) + \frac{\partial I}{\partial [\alpha/\text{Fe}]} \delta [\alpha/\text{Fe}] + \frac{\partial I}{\partial [\text{C}/\text{H}]} \delta [\text{C}/\text{H}], \quad (5)$$

where the partial derivatives are derived by the models and the observed variation δI is obtained with respect to a reference point. Our use of a linear combination of model parameters is justified in Fig. 9 where we see that the index variations are indeed linear with respect to changes in the model parameters in equation (5). For a given observed data point, by considering any number of indices larger than four at once, we can perform a multiregression analysis and obtain the corresponding variations of $\delta \log(t)$, $\delta \log(Z)$, $\delta [\alpha/\text{Fe}]$ and $\delta [\text{C}/\text{H}]$. For the purposes of the regression analysis, we have first considered the whole sample regardless of environment and then two subsamples chosen to be representatives of the ‘field’ and ‘cluster’ environment. For the field subsample, we take $1/r_5 \leq 0.5$ and for the cluster subsample, we take $1/r_5 \geq 1.5$. We then bin the index data in σ . Index variations are computed relative to the index values for the whole sample at $\sigma = 200 \text{ km s}^{-1}$.

In a preliminary analysis, we have not considered the variation of the abundance of carbon $[\text{C}/\text{H}]$. This allows a comparison of the results obtained with our new models with those obtained with the models of Thomas et al. (2004). The outcome of this analysis can be summarized as follows. Although we always find an α -enhancement that increases with velocity dispersion, our results for the age and metallicity depend on which indices are included in the analysis. The results are similar if we make use of the models of Thomas et al. (2004). Specifically, our results change with the inclusion/exclusion of indices which have a strong dependence on the carbon abundance such as C4668 and Mg1. As we noted above, the lack of strong C4668– σ relation suggests that the index does not trace overall metallicity any more than the mean iron abundance. The different sensitivities specifically to carbon abundance of many of the indices make the consideration of this element of particular importance. We therefore subsequently modified our analysis to include independently the effects of carbon enhancement. Although the correction for carbon abundance is really just the most important part of a correction that should take account of other elements such

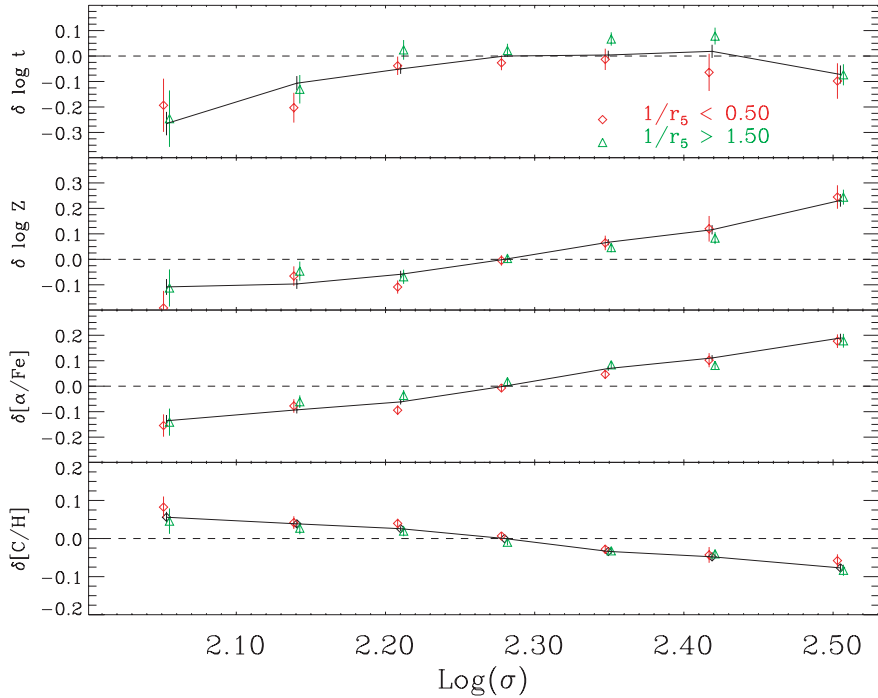


Figure 10. Age, metallicity, α -enhancement and carbon enhancement variations as a function of velocity dispersion. A linear regression analysis has been carried out simultaneously on the H β , H δ , Mg1, Mg2, Mgb, Fe4383, Fe4531, Fe5270, Fe5335, G4300 and C4668 indices. The solid line represents the entire sample, diamonds only those objects in low-density environments ($1/r_5 < 0.5$) and triangles only those in high-density environments ($1/r_5 > 1.5$). Values are differences with respect to those of the entire sample at a velocity dispersion of 200 km s^{-1} . The number of objects in each bin in σ is shown in Fig. 11

as titanium and sodium, we consider here the refinement only for carbon. As a consequence of the modification, our results for the age and metallicity using the refined model are much less dependent on the indices included in the regression analysis. With this modified model, we can include a larger number of indices and exclude only those which have a relatively strong dependence on elements not explicitly modelled (e.g. NaD, TiO1,2).

The results of this analysis are shown in Figs 10, 11 and 12. Fig. 10 shows the run of the physical parameters, expressed as differentials from the reference point. In this figure, the solid line indicates the full sample, while triangles and diamonds represent high- and low-density samples, respectively. Fig. 12 compares the values of the model indices with the observed values, for the full sample. The

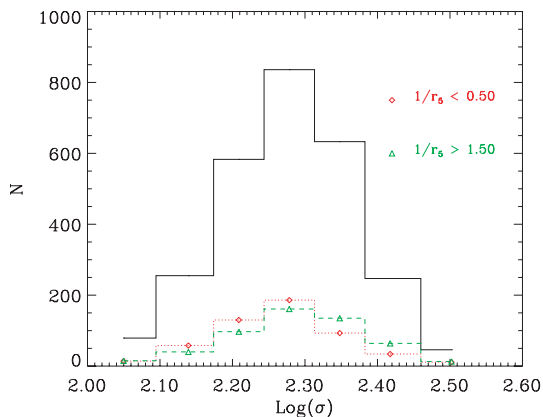


Figure 11. The number of objects in each bin of Fig. 10. The symbols have the same meanings as in Fig. 10.

model indices have been obtained by adding the model solutions found via equation (5) to the reference indices. In other words, the lines shown in Fig. 12 represent the simultaneous solution to the whole set of indices.

We note immediately that only the age is influenced by the density of environment; metallicity, $[\alpha/\text{Fe}]$ and $[\text{C}/\text{H}]$ show no dependence on environment. We find the following trends with velocity dispersion.

For the sample as a whole (solid line in Fig. 10), the age rises significantly from -0.25 dex at 100 km s^{-1} to a maximum near 260 km s^{-1} . Neither Kuntschner et al. (2001) nor Annibali et al. (2004) found any dependence of age on $\log(\sigma)$, whereas Thomas et al. (2005) found a significant positive slope ($\simeq 0.24\text{--}0.32$). Beyond 260 km s^{-1} , there is then a slight fall to -0.07 dex in the last bin at 320 km s^{-1} , significant at about the 2σ level. This decrease is more significant for galaxies in dense environments. If this decrease is real, it may be evidence that the most massive galaxies in dense environments have undergone some recent star formation.

In the range $140\text{--}260 \text{ km s}^{-1}$, galaxies in low-density environments are $\simeq 0.07$ dex (~ 1.5 Gyr for an elliptical of 10 Gyr) younger than their counterparts in dense environments for a given σ . Although the significance of this difference is low in any single bin in velocity dispersion the consistency of the difference is evidence that it is a real difference. This result is almost independent of the models adopted and, since the comparison is performed at fixed σ , it is also unlikely to be affected by the velocity dispersion correction or the reference to the Lick system.

The metallicity shows a very significant, monotonic rise from -0.1 dex at 100 km s^{-1} to $+0.25$ at 320 km s^{-1} described well by

$$\frac{d \log(Z)}{d \log(\sigma)} \simeq 0.76, \quad (6)$$

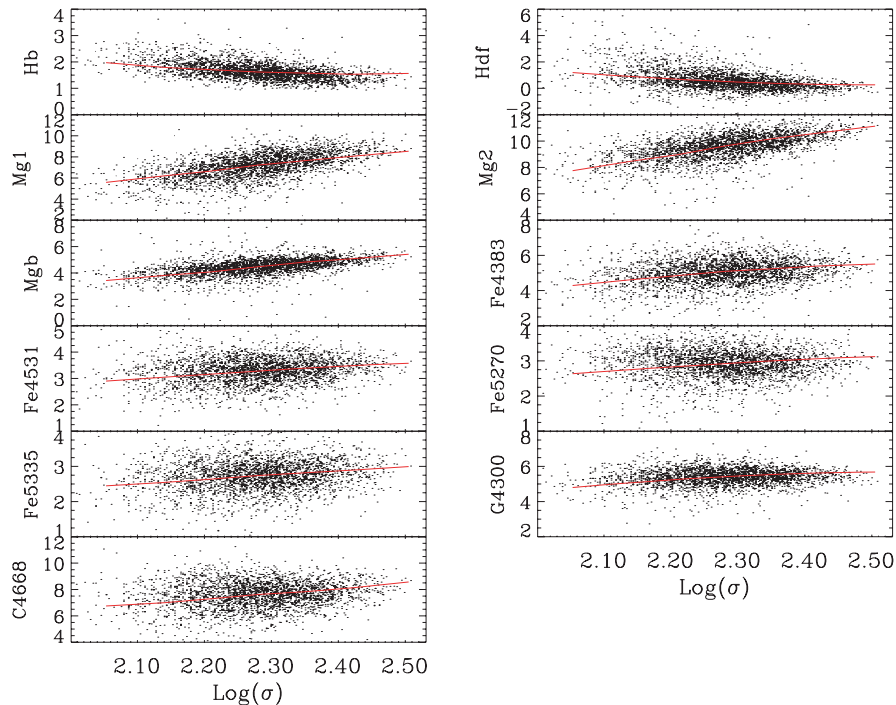


Figure 12. A posteriori comparison of the models used in the regression analysis of Fig. 10 with the indices included in the analysis. The lines are the simultaneous solution to the whole set of indices.

and independent of environment. This is in good agreement with the value found by Kuntschner et al. (2001). It is 20 per cent larger than that derived by Annibali et al. (2004), 30 per cent larger than that found by Nelan et al. (2005) and 40 per cent larger than that of Thomas et al. (2005). Although in this latter case the models show a zero-point offset in metallicity with respect to those used in this study, this should not result in a different gradient in the differential analysis carried out here. It is more likely that the difference is due to differences in aperture or velocity dispersion corrections. Bernardi et al. (2006) found values in the range 0.38–0.58, again somewhat lower than our value.

The α -enhancement rises from -0.15 dex to $+0.2$ dex from 100 to 320 km s^{-1} . We fit the linear relation

$$\frac{d[\alpha/\text{Fe}]}{d \log(\sigma)} \simeq 0.74. \quad (7)$$

This slope is about 1.5 times that found by Annibali et al. (2004) and about 2.5 times larger than that found by Thomas et al. (2005) and Kuntschner et al. (2001). It is also a factor of 2 steeper than that found by Bernardi et al. (2006) and Nelan et al. (2005). This chemical-enrichment pattern shows that the star formation process in low-mass haloes has occurred over a longer time-scale, showing that the effect of feedback must be important in the baryon assembly process. Whatever the details of this feedback, environment has no role to play.

The carbon enhancement instead shows a steady fall from $+0.05$ dex to -0.075 dex from the lowest to the highest velocity dispersion:

$$\frac{d[\text{C}/\text{H}]}{d \log(\sigma)} \simeq -0.31. \quad (8)$$

For more massive galaxies carbon is underproduced relative to other metals. This is the first time that such a trend can be quantified.

We see from Fig. 12 that despite the trends seen with velocity dispersion in Fig. 10, there is none the less a large spread in the index values for any given value of σ . Therefore, there exist galaxies with $\sigma \sim 100 \text{ km s}^{-1}$ that are as old and metal rich as those with $\sigma \sim 300 \text{ km s}^{-1}$. However, the fact that the range of $H\beta$ and $H\delta$ values is much smaller at large velocity dispersion than at low velocity dispersion is evidence that the converse is not true: galaxies with $\sigma \sim 300 \text{ km s}^{-1}$ are never as young and metal poor as the typical galaxy with $\sigma \sim 100 \text{ km s}^{-1}$.

5 DISCUSSION

The current sample of early-type galaxies has been selected in such a way as to avoid the redshift/density bias that is introduced by traditional selection techniques when applied to a survey with a limited sky coverage. With a sample so defined, we find that there is no difference in either the redshift distribution or the z -band luminosity distribution of early-type galaxies in more- or less-dense environments. We do, however, find that environment affects the distribution of velocity dispersion, with the mean σ rising with the local density of the environment. This permits the analysis of the sample as a whole without considering separate bins of either redshift or galaxy luminosity, and the consideration only of the distribution of σ within restricted ranges. Furthermore, the large number of galaxies allows a robust estimate of the mean values of the indices at increasing velocity dispersion, even when subsamples of objects belonging to different environments are selected. In fact the presence of environmental effects has already been qualitatively inferred from the statistical analysis described in Section 4.2.

From the quantitative analysis performed with new models, in which we have included all the major dependencies from the physical parameters, we infer that both the enhancement of α -elements and the global metallicity increase with galactic velocity dispersion. Instead, contrary to previous studies, we find that the age initially

increases but then flattens, and possibly then falls at the highest velocity dispersions.

While some of these trends have already been uncovered by previous studies (Bressan, Chiosi & Tantalo 1996; Thomas et al. 2005), it is only by means of a careful statistical analysis of a large data sample and its interpretation with the most up-to-date SSPs presented here, that it is possible to obtain perhaps the cleanest scenario so far for the formation and evolution of early-type galaxies in different environments. Despite broad agreement with recent studies based on similarly large samples (Nelán et al. 2005; Bernardi et al. 2006; Smith et al. 2006), one key difference emerges; that is, our finding that the *only* environment sensitive parameter is age. The above authors also found slightly enhanced α abundances in denser environments. Whether this difference is a result of sample selection criteria or diverse approaches to data analysis is not clear.

The general picture which emerges from our work is that at fixed mass (σ), galaxies formed first in dense environments (that now correspond to clusters) and ~ 1.5 Gyr later in the less-dense field, but with a similar star formation time-scale. If the early collapse in high-density peaks happened at a redshift of, say, $z \geq 6$, then a 1.5-Gyr delay is compatible with a late collapse at redshift of $z \simeq 2.5$. Lower mass galaxies ($\sigma \simeq 100 \text{ km s}^{-1}$) formed ~ 4 Gyr more recently in both environments, which would correspond to a mean formation redshift of ~ 1.1 if those with $\sigma \simeq 220 \text{ km s}^{-1}$ formed at $z = 6$. The star formation rate that characterized the mass assembly was more rapid for more massive objects (from the increase in $[\alpha/\text{Fe}]$ with σ).

The observations are at odds with the predictions of usual hierarchical models of galaxy formation, where smaller haloes typically collapse earlier than the larger ones (Lacey & Cole 1994), indicating that an important ingredient is still missing in these models. If we assume a standard initial mass function (IMF), that is, not biased towards high-mass stars, the trend of α -enhancement with velocity dispersion suggests that the stars that make up more massive early-type galaxies formed over characteristically shorter time-scales than those that make up lower mass objects. Furthermore, in the absence of an effect of environment on the α -enhancement, we are led to conclude that the time-scale of a typical star formation episode is not affected directly by the environment, only by the mass of the object in question. Since at constant efficiency the metal enrichment is larger when the star formation process lasts longer, this implies that the baryon assembly must have been much less efficient in smaller systems. This is strong evidence for the importance of the energetic feedback on the star formation process, as recently shown by Granato et al. (2004). In these models, the star formation process in smaller systems is rendered less efficient by the supernova feedback with the result that, though starting earlier, the star formation lasts longer, giving rise to a lower metal enrichment.

Although slower star formation with stronger feedback in low-mass systems explains the observed trends in metallicity and α -enhancement, it does not get over the problem of how most of the star formation occurred after the mass was assembled. If this were not the case, we would not observe a rising $[\alpha/\text{Fe}]$ with velocity dispersion. Given that gas-rich mergers are expected to be accompanied by bursts of star formation, it is difficult to see how the star formation can be delayed if multiple-mergers are responsible for the mass assembly. Conversely, a small number of mergers would produce systems with a significant net angular momentum.

It is not possible from the present analysis to quantify the effects of major mergers, though their efficiency should be higher in the kind of low-velocity encounter typical of the field than in the high-velocity encounters expected in clusters. It could then also be possible that the formation process in field early-type galaxies is modulated by

the occurrence of major mergers. Annibali et al. (2004) have shown that in that case the fraction of stars formed during the burst is less than 25 per cent.

Finally, we find that $[\text{C}/\text{H}]$ decreases at increasing metal content. This carbon anomaly is suggested by comparison of observed index values (Fig. 8) and is thus independent of the models.

Models in which $[\text{C}/\text{H}]$ scales with the metal content do not provide consistent results between indices with different sensitivity to this element. The variation of $[\text{C}/\text{H}]$ between low- and high- σ galaxies is approximately 0.125 dex, independent of environment. It is worth noting that several indices, usually adopted for this kind of theoretical analysis, have a more- or less-pronounced dependence on the carbon abundance (including Mg1, Mg2 and to a lesser extent Mgb, see e.g. Korn et al. 2005). It is thus important to perform the analysis with suitable models that account for this effect. This abundance trend may suggest a lower production of carbon in more-metal-rich, high-mass stars. But it may also indicate a lower C yield from intermediate-mass stars as the ‘hot bottom burning’ process becomes more efficient at increasing metal content (Marigo, Bressan & Chiosi 1998)

6 CONCLUSIONS

We have carried out a detailed analysis of the spectral line indices of a sample of 3614 early-type galaxies selected from the SDSS. Our selection technique avoids the redshift/environment bias introduced by traditional selection criteria when applied to a survey with partial sky coverage. We have quantified the density of environment for each object and have investigated the effects of environment on age, metallicity and α -enhancement via a regression analysis of the whole sample. Because the carbon abundance has a strong effect on the strength of many indices we have used revised models which take account of also the carbon abundance explicitly. Thus, our models take into account the main parameters that drive the set of indices adopted in the analysis: age, metallicity, α -enhancement and carbon content.

Our results for early-type galaxies can be summarized as follows.

- (i) Neither the z -band luminosity nor the redshift distribution is a function of galaxy environment out to a redshift of 0.1.
- (ii) The mean velocity dispersion is higher in denser environments.
- (iii) The only effect of environment is on the mean age of early-type galaxies for a given velocity dispersion. Environment has no effect on metallicity, α -enhancement or $[\text{C}/\text{H}]$.
- (iv) The star formation episodes responsible for the assembly of the baryonic mass of early-type galaxies were of shorter duration in objects which have a higher present-day mass. Environment did not influence the duration of these episodes.
- (v) The youngest objects are those with the lowest masses, in both high- and low-density environments.
- (vi) Objects in the field with all but the highest velocity dispersion are, on average, 1.5 Gyr younger than their cluster counterparts. The same trend is also obtained by adopting the models by Thomas et al. (2005).
- (vii) Carbon becomes increasingly underabundant in higher mass objects.

The trend we find of increasing α -enhancement with galaxy mass is consistent with a pure monolithic collapse model. However, the more prolonged star formation in lower mass objects should also produce a higher metallicity in these objects, which is not seen. A pure monolithic collapse model is therefore rejected. In a

simple hierarchical merger scenario, the α -enhancement trend is not reproduced. The α -enhancement trend could be explained in a hierarchical model if small-mass haloes, which formed within a large dark matter halo, formed their stars more rapidly than equivalent-mass objects in a smaller parent halo. However, such a picture would predict a dependency of the star formation time-scale (and thus α -enhancement) also on environment. We see no such effect with environment. Galaxy formation in which the star formation process is dependent only on the mass of the galaxy is not consistent with either simple monolithic collapse or hierarchical merging.

A rising α -enhancement and metallicity with velocity dispersion requires a feedback mechanism that results in (i) a slower star formation in low-mass objects, and (ii) a less-efficient star formation in low-mass objects. The latter ensures that the more prolonged star formation in low-mass objects does not result in more metals. A model with mass-dependent feedback has been investigated by Granato et al. (2004).

Small-mass haloes then, can collapse before larger mass haloes, only if the star formation within them is inhibited by such a feedback mechanism, such that, in the absence of mergers, their star formation proceeds at an extremely slow rate. When mergers take place, the increased mass reduces the feedback, and the rate and efficiency of star formation increase. The greater the merger mass, the more the star formation rate is increased and the sooner it ends. The result is that the mean age of the stars formed increases with mass even though the merger epoch can be earlier for lower mass systems. There is therefore an important distinction between the epoch of assembly of the dark halo and the mean age of the stars in a galaxy which we measure spectroscopically. The difference is largest for low-mass galaxies. In environments with a high density, the merger process occurred ~ 1.5 Gyr earlier than in low-density environments and this timing seems to be the only influence of the environment.

ACKNOWLEDGMENTS

MSC thanks the Istituto Nazionale di Astrofisica for support in the form of a Research Fellowship. We also thank L. Danese for useful discussions. We are grateful to an anonymous referee whose prompt comments led to a substantial improvement of this paper.

Funding for the creation and distribution of the SDSS Archive has been provided by the Alfred P. Sloan Foundation, the Participating Institutions, the National Aeronautics and Space Administration, the National Science Foundation, the US Department of Energy, the Japanese Monbukagakusho, and the Max Planck Society. The SDSS Web site is <http://www.sdss.org/>.

The SDSS is managed by the Astrophysical Research Consortium (ARC) for the Participating Institutions. The Participating Institutions are The University of Chicago, Fermilab, the Institute for Advanced Study, the Japan Participation Group, The Johns Hopkins University, the Korean Scientist Group, Los Alamos National Laboratory, the Max-Planck-Institute for Astronomy (MPIA), the Max-Planck-Institute for Astrophysics (MPA), New Mexico State University, University of Pittsburgh, University of Portsmouth, Princeton University, the United States Naval Observatory, and the University of Washington.

REFERENCES

Annibali F., Danese L., Rampazzo R., Bressan A., Bertone E., Chavez M., Zeilinger W. W., 2004, in Dettmar R., Klein U., Salucci P., eds, *Baryons in Dark Matter Halos*. SISSA, Trieste, p. 56
 Balogh M. et al., 2004, *MNRAS*, 348, 1355

Balogh M. L., Morris S. L., Yee H. K. C., Carlberg R. G., Ellingson E., 1999, *ApJ*, 527, 54
 Bender R., Burstein D., Faber S. M., 1993, *ApJ*, 411, 153
 Bernardi M., Sheth R. K., Nichol R. C., Schneider D. P., Brinkmann J., 2005, *AJ*, 129, 61
 Bernardi M., Nichol R. C., Sheth R. K., Miller C. J., Brinkmann J., 2006, *AJ*, 131, 1288
 Bernardi M., Renzini A., da Costa L. N., Wegner G., Alonso M. V., Pellegrini P. S., Rit e C., Willmer C. N. A., 1998, *ApJ*, 508, L143
 Bernardi M. et al., 2003, *AJ*, 125, 1882
 Bower R. G., Lucey J. R., Ellis R. S., 1992, *MNRAS*, 254, 601
 Bressan A., Chiosi C., Tantalo R., 1996, *A&A*, 311, 425
 Burstein D., Faber S. M., Gaskell C. M., Krumm N., 1984, *ApJ*, 287, 586
 Cappellari M. et al., 2006, *MNRAS*, 366, 1126
 Croton D. J. et al., 2005, *MNRAS*, 356, 1155
 Denicol  G., Terlevich R., Terlevich E., Forbes D. A., Terlevich A., 2005, *MNRAS*, 358, 813
 Dressler A., 1980, *ApJ*, 236, 351
 Fukugita M., Peebles P. J. E., 2004, *ApJ*, 616, 643
 G mez P. L. et al., 2003, *ApJ*, 584, 210
 Gonz lez J., 1993, PhD thesis, Univ. California, Santa Cruz
 Goto T., Yamauchi C., Fujita Y., Okamura S., Sekiguchi M., Smail I., Bernardi M., G mez P., 2003, *MNRAS*, 346, 601
 Granato G. L., De Zotti G., Silva L., Bressan A., Danese L., 2004, *ApJ*, 600, 580
 Gunn J. E., Gott R., 1972, *ApJ*, 176, 1
 Hamilton D., 1985, *ApJ*, 297, 371
 Hogg D. W. et al., 2003, *ApJ*, 585, L5
 Hogg D. W. et al., 2004, *ApJ*, 601, L29
 Jorgensen I., 1997, *MNRAS*, 288, 161
 Korn A. J., Maraston C., Thomas D., 2005, *A&A*, 438, 685
 Kuntschner H., Smith R. J., Colless M., Davies R. L., Kaldare R., Vazdekis A., 2002, *MNRAS*, 337, 172
 Kuntschner H., Lucey J. R., Smith R. J., Hudson M. J., Davies R. L., 2001, *MNRAS*, 323, 615
 Lacey C., Cole S., 1994, *MNRAS*, 271, 676
 Longhetti M., Bressan A., Chiosi C., Rampazzo R., 2000, *A&A*, 353, 917
 Maraston C., Greggio L., Renzini A., Ortolani S., Saglia R. P., Puzia T. H., Kissler-Patig M., 2003, *A&A*, 400, 823
 Marigo P., Bressan A., Chiosi C., 1998, *A&A*, 331, 564
 McIntosh D. H., Rix H.-W., Caldwell N., 2004, *ApJ*, 610, 161
 Miller C. J., Nichol R. C., G mez P. L., Hopkins A. M., Bernardi M., 2003, *ApJ*, 597, 142
 Moore B., Katz N., Lake G., Dressler A., Oemler A., Jr, 1996, *Nat*, 379, 613
 Nelan J. E., Smith R. J., Hudson M. J., Wegner G. A., Lucey J. R., Moore S. A. W., Quinney S. J., Suntzeff N. B., 2005, *ApJ*, 632, 137
 Nikolic B., Cullen H., Alexander P., 2004, *MNRAS*, 355, 874
 Puzia T. H., Saglia R. P., Kissler-Patig M., Maraston C., Greggio L., Renzini A., Ortolani S., 2002, *A&A*, 395, 45
 Rampazzo R., Annibali F., Bressan A., Longhetti M., Padoan F., Zeilinger W. W., 2005, *A&A*, 433, 497
 Rose J. A., 1984, *AJ*, 89, 1238
 Rose J. A., 1985, *AJ*, 90, 1927
 S nchez-Bl zquez P., Gorgas J., Cardiel N., Cenarro J., Gonz lez J. J., 2003, *ApJ*, 590, L91
 Shimasaku K. et al., 2001, *AJ*, 122, 1238
 Smith R. J., Hudson M. J., Lucey J. R., Nelan J. E., Wegner G. A., 2006, *MNRAS*, 369, 1419
 Strauss M. A. et al., 2002, *AJ*, 124, 1810
 Thomas D., Maraston C., Bender R., de Oliveira C. M., 2005, *ApJ*, 621, 673
 Thomas D., Maraston C., Korn A., 2004, *MNRAS*, 351, L19
 Thomas D., Maraston C., Bender R., 2003, *MNRAS*, 339, 897
 Trager S. C., Faber S. M., Worthey G., Gonz lez J. J., 2000, *AJ*, 120, 165
 Trager S. C., Worthey G., Faber S. M., Burstein D., Gonzalez J. J., 1998, *ApJS*, 116, 1
 Tripcico M. J., Bell R. A., 1995, *AJ*, 110, 3035
 Worthey G., Ottaviani D. L., 1997, *ApJS*, 111, 377
 Worthey G., Faber S. M., Gonzalez J. J., Burstein D., 1994, *ApJS*, 94, 687

APPENDIX A: ROBUSTNESS OF RESULTS TO VELOCITY DISPERSION CORRECTION OF INDICES

Our findings, that the index values for early-type galaxies are affected by environment, are not due to an error in our velocity dispersion

correction. If an error in velocity dispersion correction introduced an erroneous gradient component into the index- σ relations, this would not alter the separation between the two lines in Fig. 8, because the Monte Carlo simulations use the *measured* index- σ relations in order to establish how values of σ are translated into values of the index. In order to show this, we carried out two tests. In the first, we introduced an error term into the gradient of the

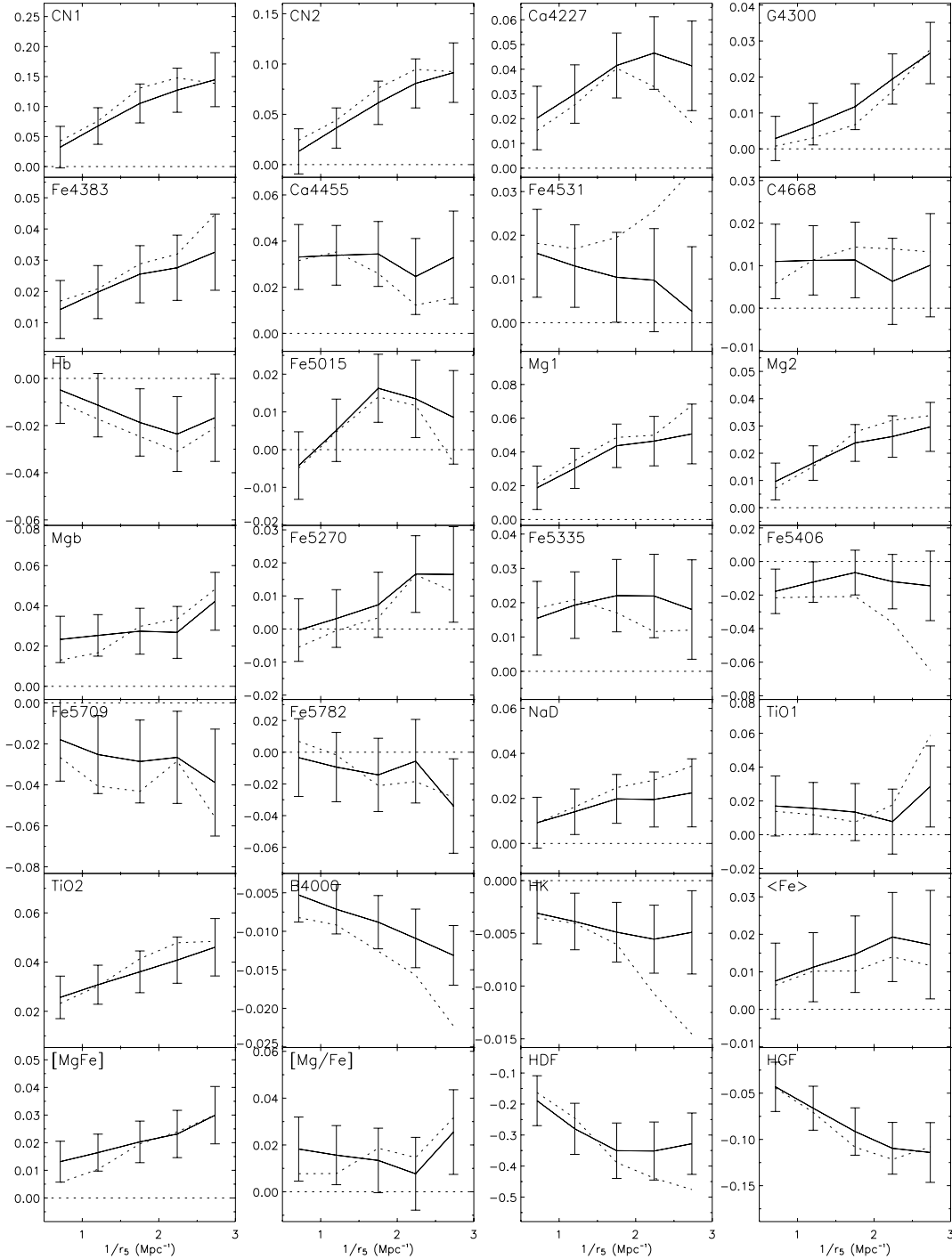


Figure A1. Effect of environment on relative line index strength free of the effect of the index- σ relation. Similar to Fig. 8 but shown is the difference between the data and simulation. The solid line is for the subsamples exactly as defined in Fig. 8 and the dotted line is for subsamples which have been constrained (by random sampling in bins of σ) to have similar velocity dispersion distributions. The error bars are not shown for the second line but are similar to those of the solid line. The similarity of the lines shows that neither an error in velocity dispersion correction nor the differences in velocity dispersion distribution between subsamples can explain the effect we find with environment.

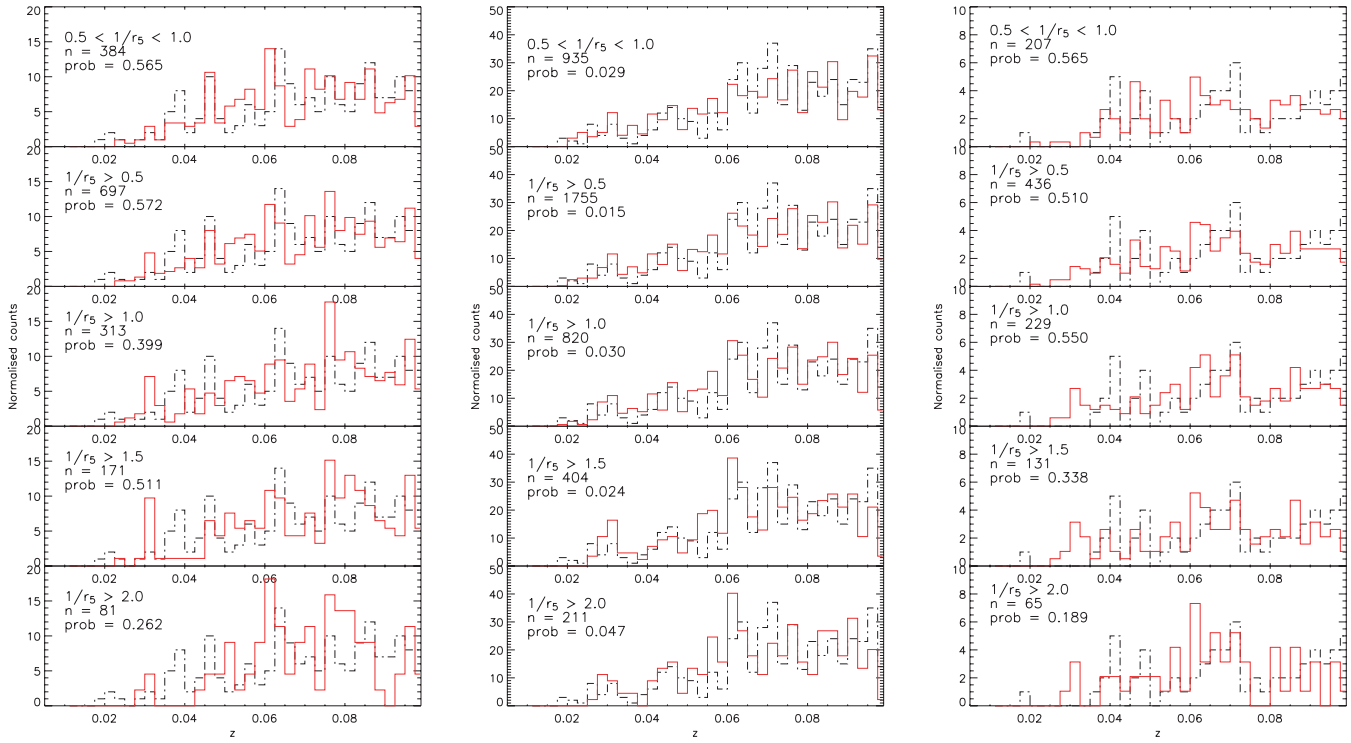


Figure A2. Distribution of redshift for various density environments for three ranges of the velocity dispersion. The lines and labelling are as in Fig. 6. Left-hand panel: $\sigma < 160 \text{ km s}^{-1}$, middle panel: $160 \leq \sigma \leq 230 \text{ km s}^{-1}$, right-hand panel: $\sigma > 230 \text{ km s}^{-1}$. The curves are normalized to the number of objects in the low-density comparison sample which contains 185, 473 and 68 objects, respectively, for the three ranges.

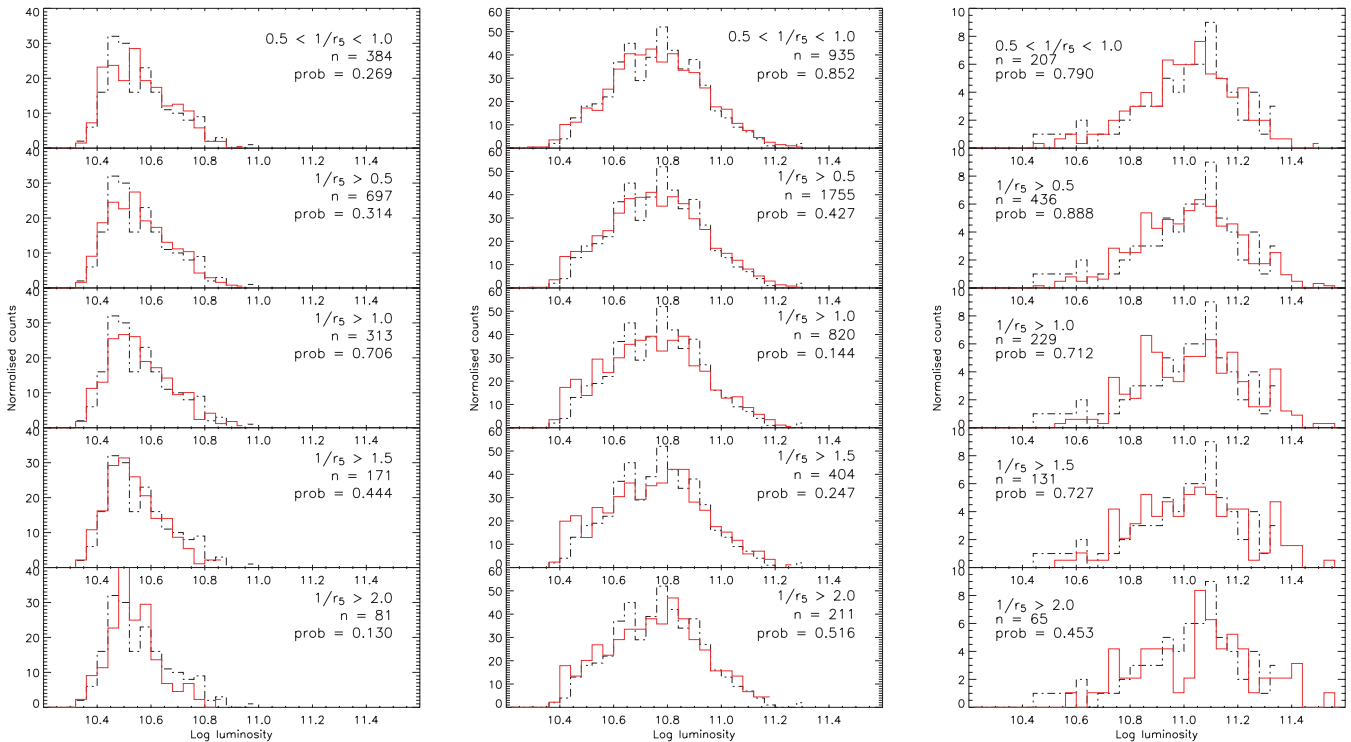


Figure A3. Same as Fig. A2 but for the distribution of luminosity.

index– σ relations and re-computed the simulations illustrated in Fig. 8. No differences were seen that extended beyond the error bars in this figure. Secondly, we constrained the σ -distributions of the subsamples in each environment to be identical to that of the comparison subsample ($1/r_5 < 0.5$) by randomly selecting objects until the number of objects per bin was in constant proportion to the numbers in the comparison sample. This, of course, leads to the exclusion of many objects but as this is at random, only the size of the errors on individual points will be affected. Reproducing Fig. 8 in this way also did not change the index difference between data and simulations. The results of this test are shown in Fig. A1 where we have subtracted the simulation from the data to illustrate the effect of environment alone on the line indices. In short, our results on the effect of environment are robust to errors in velocity dispersion correction because it is not dependent on the form of the index– σ relation.

In order to test whether these differences affect only the low-mass objects or are general to the early-type population as a whole (at least for objects brighter than -20.45 in R -band), we have repeated our analysis for three bins in velocity dispersion chosen to represent low-, intermediate- and high-mass systems: $\sigma < 160 \text{ km s}^{-1}$, $160 \leq \sigma \leq 230 \text{ km s}^{-1}$ and $\sigma > 230 \text{ km s}^{-1}$, respectively. The redshift and

luminosity distributions of these subsamples are shown in Figs A2 and A3, where it can be seen that they are similarly distributed. The results of the analysis for these three ranges of velocity dispersion are shown in the rightmost three panels for each index of Fig. 8.

Bearing in mind the larger errors on the results for the sample when divided by velocity dispersion (especially for the low and high sigma subsamples), we find that most of the trends seen for the sample as a whole are also seen for the subsample with $\sigma < 160 \text{ km s}^{-1}$. Indeed, the magnitude of the environmental index differences is larger for these low-mass objects for all the indices in which some effect is seen for the sample as a whole. The subsample with $\sigma > 230 \text{ km s}^{-1}$ shows effects with environment that are generally weaker than those for the low-mass subsample and for the sample as a whole such that the magnitude of the environmental effect falls from panel 2 to panel 4 of Fig. 8. CN1 and Mg1 show this trend especially clearly. However there are exceptions to this trend. G4300, Hb, Fe5015 and Fe5270 seem to show stronger trends with environment for more massive objects although none of the trends are as convincing as those in the opposite sense.

This paper has been typeset from a $\text{\TeX}/\text{\LaTeX}$ file prepared by the author.